ENHANCED CONFINED MICROWAVE TRANSMISSION BY SINGLE SUBWAVELENGTH APERTURES

A THESIS

SUBMITTED TO THE DEPARTMENT OF PHYSICS

AND THE INSTITUTE OF ENGINEERING AND SCIENCE

OF BILKENT UNIVERSITY

IN PARTIAL FULFILLMENT OF THE REQUIREMENTS

FOR THE DEGREE OF

MASTER OF SCIENCE

By

Hümeyra Çağlayan

August 2005

I certify that I have read this thesis and that in my opinion it is fully adequate, in scope and in quality, as a thesis for the degree of Master of Science.

Prof. Dr. Ekmel Özbay (Advisor)

I certify that I have read this thesis and that in my opinion it is fully adequate, in scope and in quality, as a thesis for the degree of Master of Science.

Asst. Prof. Hilmi Volkan Demir

I certify that I have read this thesis and that in my opinion it is fully adequate, in scope and in quality, as a thesis for the degree of Master of Science.

Asst. Prof. Vakur B. Ertürk

Approved for the Institute of Engineering and Science:

Prof. Dr. Mehmet B. Baray
Director of the Institute Engineering and Science

ABSTRACT

ENHANCED CONFINED MICROWAVE TRANSMISSION BY SINGLE SUBWAVELENGTH APERTURES

Hümeyra Çağlayan
M.S. in Physics
Supervisor: Prof. Dr. Ekmel Özbay
August 2005

Grating-coupling phenomena between surface plasmons and electromagnetic waves are studied in the microwave spectrum using metallic circular apertures surrounded by an array of grooves. The measurements are performed in the microwave spectrum of 10-18 GHz, corresponding to a wavelength region of 16.7-30 mm. The metallic samples have a subwavelength hole with a diameter of 8 mm and have concentric grooves with a periodicity of 16 mm. We first present the experimental and theoretical results of enhanced microwave transmission though a subwavelength circular aperture with concentric periodic grooves around the surface plasmon resonance frequency. This is followed by transmission studies through circular annular apertures with and without concentric periodic grooves around the aperture. We demonstrate a 145-fold enhancement factor could be obtained with a subwavelength circular annular aperture surrounded by concentric periodic grooves. Moreover, we study the diffraction of electromagnetic waves from subwavelength metallic circular annular apertures in the microwave spectrum. The theoretical and experimental demonstration of the near- and far-field EM distributions for subwavelength circular apertures and circular annular apertures surrounded by concentric periodic grooves is reported. We present the angular transmission distributions from circular apertures and circular annular apertures surrounded by concentric periodic grooves. At the surface mode resonance frequency the transmitted electromagnetic waves from the subwavelength circular annular aperture surrounded by concentric periodic grooves have a strong angular confinement with an angular divergence of $\pm 3^o$. This represents a four-fold reduction when compared to the angular divergence of the beam transmitted

from a subwavelength aperture. These results show, that not only high transmission but also a confined beam is achieved at the surface plasmon resonance frequency using a circular annular aperture with grooves .

Keywords: surface plasmon, extraordinary transmission, plasmon coupling, grating structures, subwavelength aperture, microwave radiation, beaming.

ÖZET

DALGABOYU-ALTI DELİKLERLE YÜKSELTİLMİŞ YÖNLENDİRİLMİŞ MİKRODALGA GEÇİRGENLİK

Hümeyra Çağlayan
Fizik, Yüksek Lisans
Tez Yöneticisi: Prof. Dr. Ekmel Özbay
Ağustos 2005

Yüzey plazmonları ile elektromanyetik dalgalar arasında ızgaralar vasıtası ile elde edilen etkileşim metalik yuvarlak yarıklı etrafı yivlerle çevrili yapılar kullanılarak mikrodalga spektrumunda incelendi. Ölçümler, 16.7-30 mm dalga boyuna karşılık gelen 10-18 GHzde mikrodalga frekans aralığında yapıldı. Metal örneklerin ortasındaki deliğin çapı 8 mm ve etrafındaki içiçe geçmiş yivlerin periyodu da 16 mm'dir. Öncelikle dalgaboyu-altı delikli ve içiçe geçmiş periyodik yivleri olan yapının yüzey plazmonu rezonans frekansı etrafındaki artırılmış geçirgenlik deneysel ve kuramsal sonuçları gösterildi. Bunu halkalı yapıda ve etrafı içiçe geçmiş periyodik yivlerle kaplı halkalı yapıdaki geçirkenlik çalışmaları takip etti. Etrafı içiçe geçmiş periyodik yivlerle kaplı halkalı yapı ile 145 kat artırım elde edilebileceğini gösterdirildi. Bunlara ek olarak elektromagnetik dalgaların dalgaboyu-altı delikli metal yapılardan dağılımını inceledindi. Etrafı içiçe geçmiş periyodik yivlerle çevrili dalgaboyu-altı delikli ve halkalı yapılarda elektromagnetik dalgaların yakın ve uzak alanlardaki dağılımlarının kuramsal ve deneysel gösterimini rapor edildi. Etrafı içiçe geçmiş periyodik yivlerle çevrili dalgaboyu altı delikli ve halkalı yapılarda açısal geçirgenlik dağılımı sunuldu. Yüzey plazmonu rezonans frekansında etrafı içiçe geçmiş periyodik yivlerle çevrili dalgaboyu-altı halkalı yapıdan geçen elektromagnetik dalgaların ± 3 derecelik açısal dağılım ile çok kuvvetli bir açısal yönlendirmesi bulundu. Bu sonuç, dalgaboyu-altı delikten geçen ışının açısal dağılımına göre 4 katlık bir azalmaya karşılık gelmektedir. Bu sonuçlar, etrafı içiçe geçmiş periyodik yivlerle çevrili dalgaboyu-altı halkalı yapı ile yüzey plazmonu rezonans frekansında yüksek geçirgenliğin yanında açısal olarak yönlendirimiş bir ışın elde edilebileceğini de göstermektedir.

Anahtar sözcükler: yüzey plazmonu, artırılmış geçirgenlik, plazmon bağlama, ızgara yapılar, dalgaboyu-altı delik, mikrodalga radyasyon, yönlendirme.

Acknowledgement

I would like to express my gratitude to my supervisor Prof. Dr. Ekmel Özbay for his guidance and help in the supervision of the thesis. His personal and academic virtue greatly shaped my approach to physics and scientific study. I feel lucky to be his student.

I would like to thank to the members of my thesis committee, Asst. Prof. Hilmi Volkan Demir and Asst. Prof. Vakur B. Ertürk, for reading the manuscript and commenting on the thesis.

I would like to express my special thanks and gratitude to İrfan Bulu and Yeşim abla.

I would like to thank all members of Nanotechnology Research Center. I want to especially thank the group members of the metametarials research team: İrfan Bulu, Koray Aydın, Kaan Güven and K. Bora Alıcı. It was a pleasure to work with these hard-working friends in the same group.

Finally I would express my endless thank to my family for their understanding and continuous moral support. Very special thanks belong to my partner, Hasan, for his endless moral support, encouragement, understanding, and love.

The whole of science is nothing more than a refinement of everyday thinking.

Albert Einstein

Contents

List of Figures

Chapter 1

Introduction

Surface Plasmons (SPs) are waves that propagate along the surface of a conductor. These are essentially light waves that are trapped on the surface because of their interaction with the free electrons of the conductor. In this interaction, the free electrons respond collectively by oscillating in resonance with the light wave. The resonant interaction between the surface charge oscillation and the electromagnetic field of the light constitutes the SP and gives rise to its unique properties [1, 2, 3].

Surface plasmons are of interest to a wide class of scientists, ranging from physicists to chemists, from material scientists to biologists. Increased interest in SPs stems from the recent advances that allow metals to be structured and characterized at a nanometer scale. This enables us to control the SP properties in order to study the new aspects of their science and use them for specific applications. For instance, SPs are currently being explored for their potential in optics, magneto-optic data storage, microscopy and solar cells, as well as being used to construct sensors for detecting biologically interesting molecules.

For researchers in the field of optics, one of the most attractive aspects of SPs is the way in which they help us to concentrate and channel light using subwavelength structures. In 1998, Ebbesen *et al.* demonstrated extraordinary optical transmission (EOT) through subwavelength hole array structures [4]. Afterwards,

many theoretical and experimental studies on EOT through subwavelength apertures demonstrated that this phenomenon was due to resonant excitation of SPs by a periodic array on the surface. Different metal types [5], groove periodicity [5, 6, 7, 8], groove depth [6, 9], and aperture shapes [10] were used to analyze the EOT phenomena. Both 1-D [6, 9, 11, 12, 13] and 2-D [5, 14, 15, 16, 17] periodic surface corrugations were implemented in these studies. The optical beaming property of subwavelength apertures in metallic grating structures was previously reported in [12] and theoretically explained in [18].

In this work, we experimentally studied and numerically verified the transmission enhancement and beaming of microwave radiation through a subwavelength hole surrounded by periodic gratings. The thesis will be organized as follows: In Chapter 2, the plasma concept will be presented and the basic properties of surface plasmons will be obtained by solving Maxwell equations at the metal-dielectric interface. At the end of this chapter, excitation of non-radiative surface plasmons will be introduced by way of three different methods. In the Chapter 3, we will first present the samples used in our experiments. We will also briefly describe the experimental setup and the simulation technique used for our calculations. We will end this chapter by presenting the transmission and enhancement data for the samples. The work presented in Chapter 3 appeared as a journal article in Optics Express [19]. In the Chapter 4, we will focus on the beaming issue. We will present near- and far-field angular distributions of electromagnetic (EM) waves. Most of the results of Chapter 4 are submitted to appear as a journal article in the Journal of the Optical Society of America B (JOSA B) [20]. The thesis will conclude with the summary of our measurements and achievements and possible future research directions.

Chapter 2

Theoretical Background

In this chapter, the theoretical description of surface plasmons at an interface formed by a metal and a dielectric is based on Maxwell's equations. We first introduce the plasma concept in metals. Afterwards, with the use of Maxwell's equations, we derived the electromagnetic field of the surface plasmon propagating along the metal-dielectric interface. Finally, we present the excitation methods of non-radiative surface plasmons.

2.1 Plasma Optics

Many fundamental electronic properties of the solid state can be successfully described by the analogy of the single electrons moving in the periodic array of atoms. Another different approach to derive the properties of the solid state starts with the plasma concept: the free electrons of a metal are treated as an electron liquid with a high density of about $10^{23} cm^{-3}$, ignoring the lattice in the first approximation [2].

By this approach, the dielectric function for metals can be calculated [21]. The long wavelength dielectric response $\epsilon(\omega)$ of an electron gas is obtained from the equation of the motion of a free electron in an electric field:

$$m\frac{d^2x}{dt^2} = -eE. \tag{2.1}$$

If x and E have the time dependence $e^{-i\omega t}$, then Eq. 2.1 becomes

$$-\omega^2 mx = -eE \Rightarrow x = eE/m\omega^2 \tag{2.2}$$

The dipole moment of one electron is -$ex = -e^2E/m\omega^2$ and the polarization, defined as the dipole moment per unit volume, is

$$P = -nex = -\frac{ne^2}{m\omega^2}E, \tag{2.3}$$

where n is the electron concentration.

The dielectric function at the frequency ω is

$$\epsilon(\omega) \equiv \frac{D(\omega)}{E(\omega)} \equiv 1 + 4\pi\frac{P(\omega)}{E(\omega)} \tag{2.4}$$

The dielectric function of the free electron gas then follows from Eqs. 2.3 and 2.4:

$$\epsilon(\omega) = 1 - \frac{4\pi ne^2}{m\omega^2} \tag{2.5}$$

The **plasma frequency**, ω_p, is thus defined as

$$\omega_p^2 = 4\pi ne^2/m, \tag{2.6}$$

which makes $\epsilon \to 0$ as $\omega \to \omega_p$. Therefore, $\epsilon(\omega)$ can be written in turns of ω_p as:

$$\epsilon(\omega) = 1 - \frac{\omega_p^2}{\omega^2}, \tag{2.7}$$

as plotted in Fig. 2.1.

A plasma oscillation in a metal is the collective longitudinal excitation of the conduction electron gas. These plasma oscillations propagate through the volume of the metal. A plasmon is a quantum of such a plasma oscillation that has the energy of $\hbar\omega_p = \hbar\sqrt{4\pi ne^2/m}$.

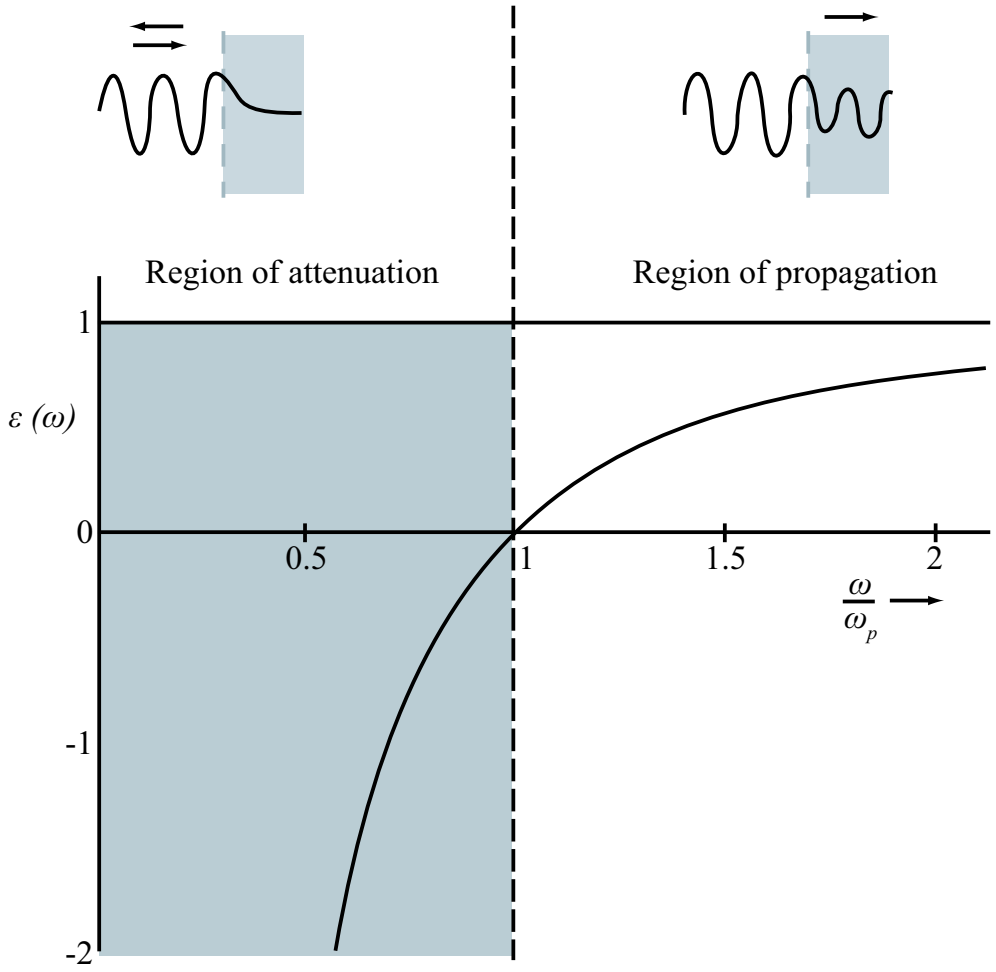

Figure 2.1: Dielectric function $\epsilon(\omega)$ of a free electron gas. Electromagnetic waves propagate without damping only when ϵ is positive and real. Electromagnetic waves are completely reflected from the medium when ϵ is negative.

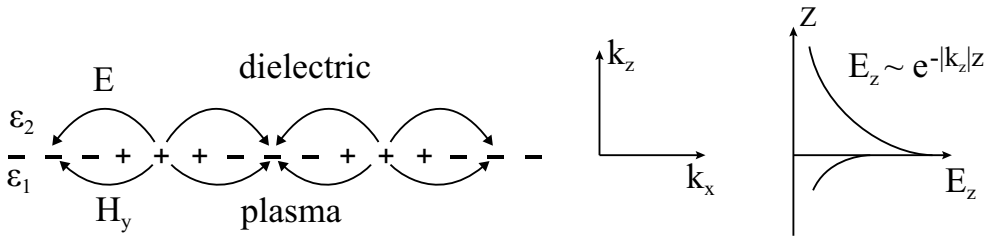

Figure 2.2: The charges and the electromagnetic field of SPs propagating on a surface in the x direction are shown schematically. The exponential dependence of the field E_z is seen on the right. H_y shows the magnetic field in the y direction for a p-polarized wave.

2.2 Plasmons at an interface: Surface Plasmons

The electron charges on a metal boundary can perform coherent fluctuations that are called surface plasma oscillations [2]. The frequency ω of these longitudinal oscillations is tied to its wavevector k_x by a dispersion relation $\omega(k_x)$. Now, we will find the wavevector of these surface waves and calculate the dispersion relation.

The layer system shown in Fig. 2.2, has an interface, between metal (ϵ_1) and air (ϵ_2) on which a p-polarization wave propagates in the x direction. There is no y dependence. We describe the fields in the media (1) and (2) as follows:

$$z < 0, H_1 = (0, H_{y1}, 0) \exp i(k_{x1}x - k_{z1}z - \omega t), \tag{2.8a}$$

$$E_1 = (E_{x1}, 0, E_{z1}) \exp i(k_{x1}x - k_{z1}z - \omega t), \tag{2.8b}$$

$$z > 0, H_2 = (0, H_{y2}, 0) \exp i(k_{x2}x + k_{z2}z - \omega t), \tag{2.8c}$$

$$E_2 = (E_{x2}, 0, E_{z2}) \exp i(k_{x2}x + k_{z2}z - \omega t), \tag{2.8d}$$

These fields have to fulfill Maxwell's equations:

$$\nabla \times H_i = \epsilon_i \frac{1}{c} \frac{\partial}{\partial t} E_i, \tag{2.9a}$$

$$\nabla \times E_i = -\frac{1}{c} \frac{\partial H_i}{\partial t}, \tag{2.9b}$$

$$\nabla . \epsilon_i E_i = 0, \tag{2.9c}$$

$$\nabla . H_i = 0, \tag{2.9d}$$

together with the continuity relations

$$H_{y1} = H_{y2}, \tag{2.10a}$$
$$E_{x1} = E_{x2}, \tag{2.10b}$$
$$\epsilon_1 E_{z1} = \epsilon_2 E_{z2}, \tag{2.10c}$$

From Eqs. 2.10a and 2.10b follows the continuity of

$$k_{x1} = k_{x2} = k_x \tag{2.11}$$

Eq. 2.9a gives:

$$\frac{\partial H_{yi}}{\partial z} = -i\epsilon_i E_{xi}\frac{\omega}{c} \tag{2.12a}$$
$$+k_{z1}H_{y1} = +\frac{\omega}{c}\epsilon_1 E_{x1} \tag{2.12b}$$
$$+k_{z2}H_{y2} = -\frac{\omega}{c}\epsilon_2 E_{x2} \tag{2.12c}$$

Eq. 2.12c together with Eqs. 2.10a and 2.10b yield

$$H_{y1} - H_{y2} = 0 \tag{2.13a}$$
$$\frac{k_{z1}}{\epsilon_1}H_{y1} + \frac{k_{z2}}{\epsilon_2}H_{y2} = 0 \tag{2.13b}$$

To obtain a solution, the determinant D_o has to be zero. Thus,

$$D_0 = \frac{k_{z1}}{\epsilon_1} + \frac{k_{z2}}{\epsilon_2} = 0 \tag{2.14}$$

This is the dispersion relation of the SPs in the system shown in Fig. 2.2 that we obtain from Eqs. 2.9a, 2.9b, and 2.12c

$$k_x^2 + k_{zi}^2 = \epsilon_i(\frac{\omega}{c})^2 \tag{2.15}$$

From Eq. 2.14 together with Eq. 2.15 follows

$$k_x = \frac{\omega}{c}(\frac{\epsilon_1\epsilon_2}{\epsilon_1 + \epsilon_2})^{1/2} \tag{2.16}$$

Since k_z is positive imaginary for electromagnetic fields which decay exponentially into the space perpendicular to the surface and have their maximum in the

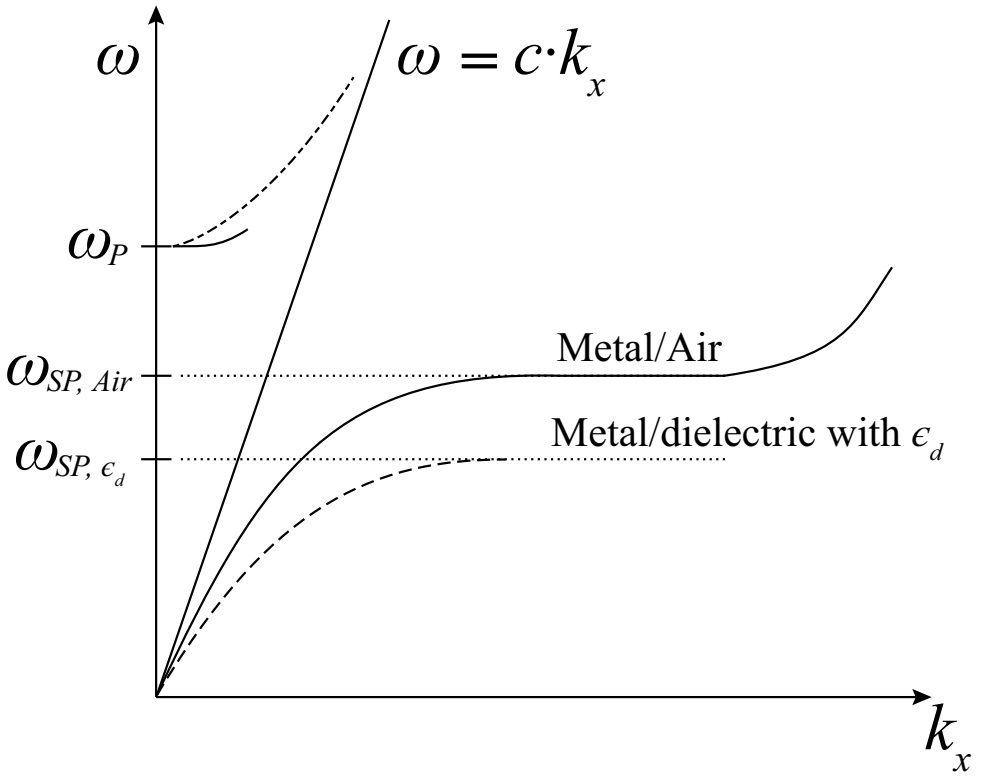

Figure 2.3: The dispersion relation of nonradiative SPs, to the right of the light line.

surface, Eq. 2.14 shows that for the surface plasmon to exist, ϵ_1 and ϵ_2 must have opposite signs:

$$\epsilon_1 \epsilon_2 < 0 \tag{2.17}$$

Also from Eq. 2.16

$$\epsilon_1 + \epsilon_2 < 0. \tag{2.18}$$

At large k_x, the value of ω approaches,

$$\omega_{sp} = \frac{\omega_p}{\sqrt{1+\epsilon_2}} \tag{2.19}$$

For an air-metal interface,

$$\omega_{sp} = \frac{\omega_p}{\sqrt{2}} \tag{2.20}$$

To illustrate these results, the dispersion curve for SPs is shown in Fig. 2.3. It can be seen that their dispersion relation $\omega(k)$ lies to the right of the light line, which means that the SPs have a longer wavevector than the light waves of the same energy $\hbar\omega$, when propagating along the surface. Therefore, they are called "non-radiative" surface plasmons, which describe the fluctuations of the surface electron density. Their electromagnetic fields decay exponentially into the space perpendicular to the surface and have their maximum in the interface, which is a typical characteristic of surface waves.

2.3 Excitation of Surface Plasmons

2.3.1 Excitation by Electrons

Electrons that penetrate into a solid transfer momentum $\hbar q$ and energy ΔE_0 to the electrons of the solid. The projection of q on the surface of the film k_x determines the wavevector and, together with the dispersion relation, the energy loss of the scattered electron $\Delta E = \hbar\omega$ (Fig. 2.4). Since the electrons are scattered at different angles θ, they transfer different momenta $\hbar k_x = \hbar k_{el}^{'} \sin\theta \cong \hbar k_{el}\theta$ with $k_{el} = 2\pi/\lambda_{el}$. If one observes the energy loss $\Delta E = \hbar\omega$ at an increasing θ, the dispersion relation of the SPs can be measured up to a large k_x value beyond the Brillouin zone.

2.3.2 Excitation by Light

The application of photons to excite SPs encounters the difficulty that the dispersion relation lies to the right of the light line ($k_x > \omega/c$). At a given photon energy $\hbar\omega$, the wave vector $\hbar\omega/c$ has to be increased by an amount of Δk_x in order to "transform" the photons into SPs. There are two methods to excite SPs by light. These are by using an ATR coupler and a grating coupler.

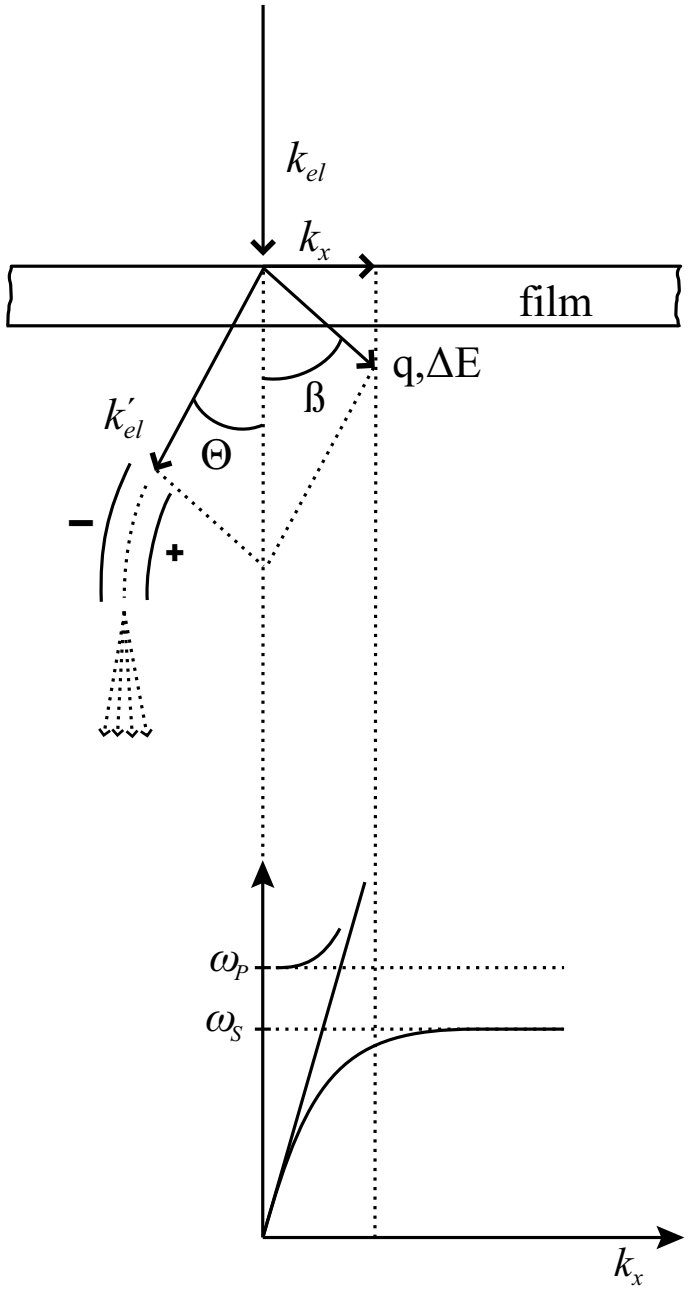

Figure 2.4: Excitation of SPs by electrons in the transmission of thin films.

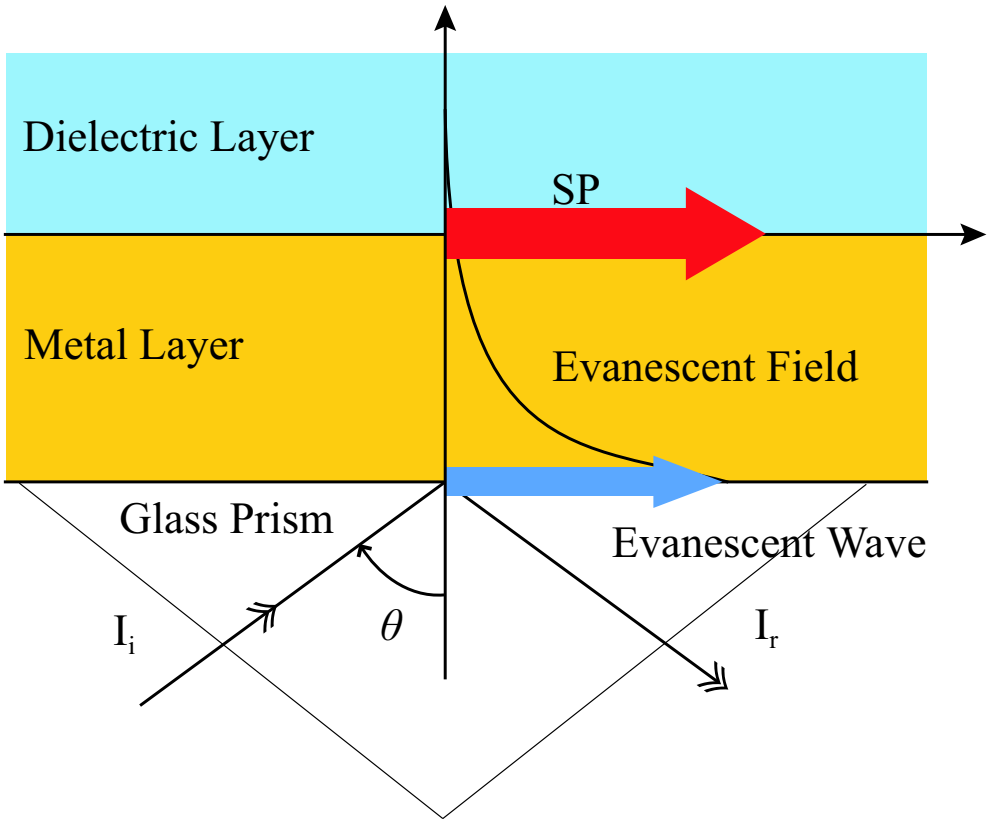

Figure 2.5: Excitation of SPs by ATR coupling.

2.3.2.1 ATR (Attenuated Total Reflection) Coupler

The basic principle of this method relies on coupling SPs with evanescent waves formed by the total internal reflection. For that, a prism is placed above the metal surface. Radiation is incident with an angle greater than the critical angle so that total internal reflection (TIR) occurs. TIR requires the evanescent modes to have a greater wavevector than the incident radiation. The tail of the evanescent mode can then excite a surface mode on the air metal surface (Fig. 2.21). The resonance condition for SPs is given by:

$$\frac{\omega}{k_x} = c\sqrt{\frac{\epsilon+1}{\epsilon}} = c/(\sqrt{\epsilon_d}\sin\theta). \tag{2.21}$$

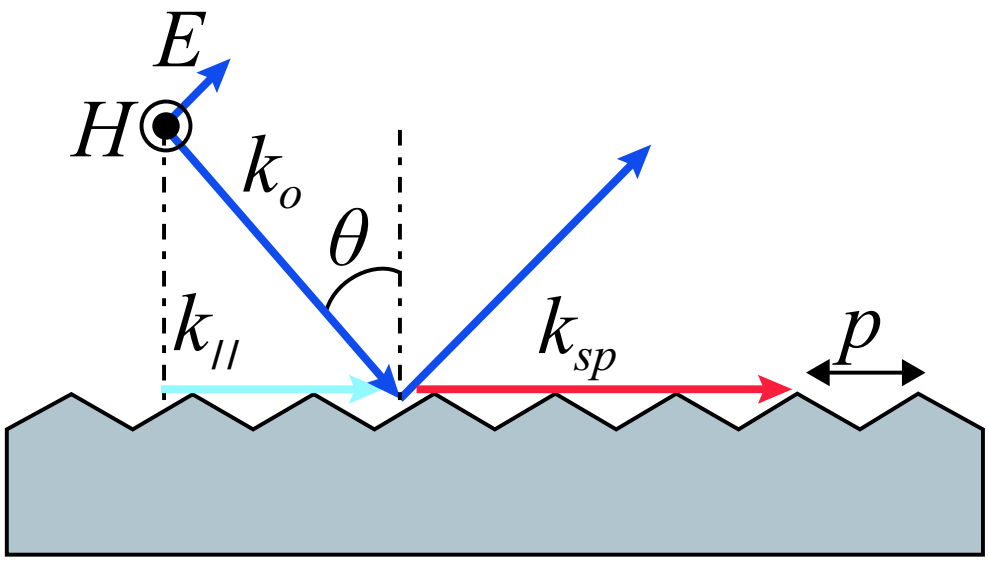

Figure 2.6: Schematic of a grating surface and k vectors.

2.3.2.2 Grating Coupler

If the incident light ($k = \omega/c$) hits a grating with a grating period (p), at an angle of θ_0 (Fig. 2.22), its component along the surface can have wavevectors given as:

$$k_{\parallel} = \frac{\omega}{c} \sin\theta_0 \pm nk_g. \tag{2.22}$$

where n is an integer and $k_g = 2\pi/p$. If $k_{\parallel}$ is equal to the wavevector of SP (Eq. 2.16), then strong coupling occurs between the incident radiation and the SP.

$$\frac{\omega}{c}\sqrt{\frac{\epsilon}{1+\epsilon}} = k_{sp} = \frac{\omega}{c} \sin\theta_0 \pm nk_g. \tag{2.23}$$

Because the grating can provide impinging free waves with additional momentum arising from the grating periodic structure, the linear free wave dispersion relation changes into a set of straight lines that can then match the SP dispersion relation (Fig. 2.7).

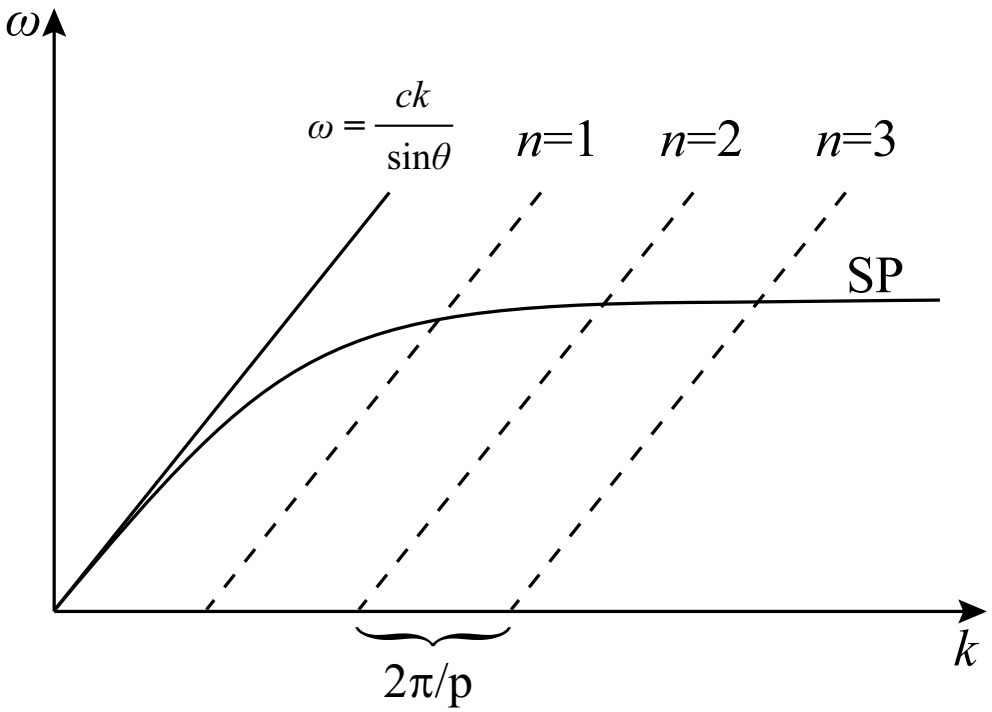

Figure 2.7: Schematic description of coupling free electromagnetic waves to SPs by the way of grating.

Chapter 3

Extraordinary Grating-coupled Transmission

3.1 Introduction

As discussed in the previous chapter, SP modes have longer wavevectors than light waves of the same energy; electromagnetic radiation does not interact with the SP modes of a smooth metal surface [2]. Therefore, the transmission of light through an aperture in a metal film is extremely small when the aperture diameter is much smaller than the wavelength. A hole structure cannot support any propagating modes and the transmission normalized to the area of the hole is proportional to $\sim (d/\lambda)^4$ where the diameter (d) of the circular hole is smaller than the wavelength (λ) of incident radiation.

However, in 1998, Ebbesen *et al.* [4] experimentally demonstrated that extraordinary transmission of light could be obtained through subwavelength hole arrays in optically thick metallic films. Not only was the transmission much larger than expected from classical diffraction theory, it was also greater than the percentage area occupied by the holes. The transmission spectra of the hole arrays displayed peaks that could be tuned by adjusting the period, nicely demonstrating the benefits that SP modes could provide.

Their results have stimulated new research dedicated to the subject of enhanced transmission. In 2002, Thio *et al.* [22] showed that a single aperture surrounded by a periodic corrugation in the metal surface could also display surface plasmon enhanced transmission. These ideas have stimulated studies on this subject and numerous experimental and theoretical works have been performed in the optical and microwave regimes [6, 13, 16, 17, 23, 24, 25, 26, 27]. In 1992, optical near-field microscope researchers proposed the use of coaxial aperture to achieve enhanced transmission [28]. Baida *et. al.* [29] proposed a similar structure that consists of subwavelength annular aperture arrays exhibiting high transmission. Theoretical simulations by this research group showed that the transmission efficiency could reach 80 % in the visible spectra range and a guided mode in the annular aperture was responsible for this large transmission [29, 30]. Recently, they also showed that it was possible to enhance the optical transmission using a subwavelength annular aperture surrounded by an array of grooves [31]. However, all of these results were theoretical predictions, and to best of our knowledge, an experimental demonstration of an enhanced transmission through a subwavelength annular aperture with concentric periodic grooves was not previously reported in the literature before this thesis work [19].

In this chapter, we experimentally study and numerically verify the enhancement of radiation through a subwavelength circular aperture surrounded by concentric periodic grooves. We also investigate high transmission assisted by the guided mode of the circular annular aperture. Furthermore, we present the extraordinary enhancement of microwave transmission through a subwavelength circular annular aperture surrounded by concentric periodic grooves. Here we show that the theoretical results are in good agreement with the experimental results.

3.2 Sample Design

We investigate the SP properties at microwave frequencies for four different samples. All of the samples are metallic and made of aluminum (Al). The samples

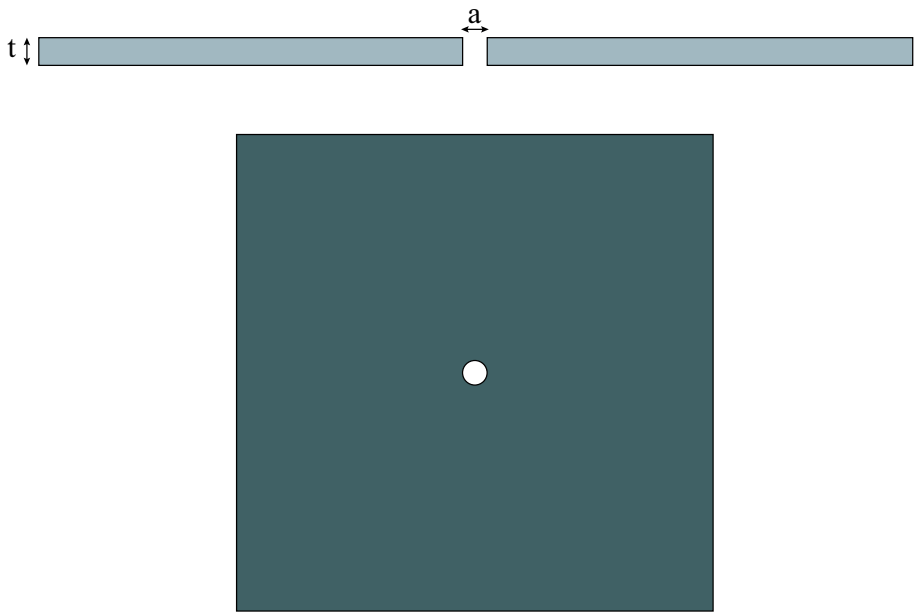

Figure 3.1: Schematic picture of a reference sample with a=8 mm and t=8 mm (Cross-sectional view on the top and front-view on the bottom).

are fabricated using a CNC machine with a process resolution of 0.1 mm.

3.2.1 Sample 1: Single Aperture (Reference Sample)

The first sample is designed as a reference sample for our measurements. We study in the frequency range of 10-18 GHz, corresponding to a wavelength region of 16.7-30 mm. Since it is known that apertures smaller than an incident wavelength transmit very poorly and diffract EM radiation in all directions, the reference sample is designed as a 25 cm×25 cm metal plate with a subwavelength hole in the center. The diameter of the hole (a) is 8 mm and the thickness of the metallic plate (t) is 8 mm (Fig. 3.1).

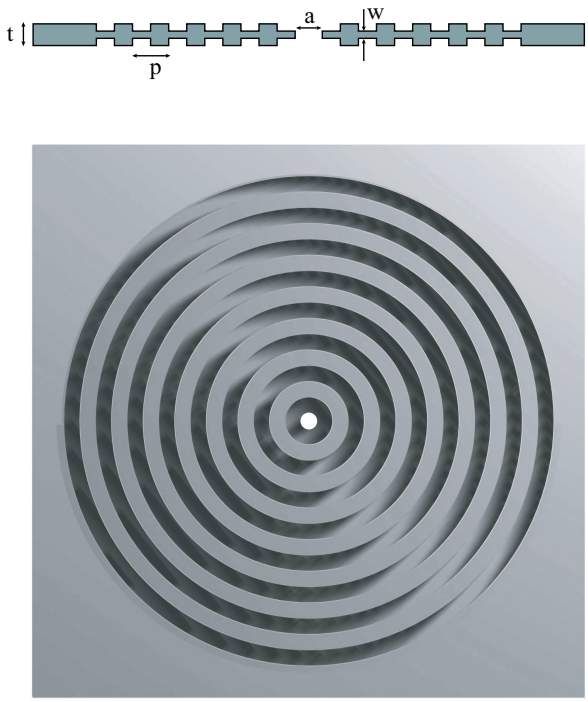

Figure 3.2: Schematic picture of Sample 2 with a=8 mm, t=8 mm, p=16 mm and w=3.2 mm (Cross-sectional view on the top and front-view on the bottom).

3.2.2 Sample 2: Aperture with periodic grooves

As explained in the theoretical background in Chapter 2, there are several methods to excite surface plasmons. Grating coupling is one of these methods and is achieved by means of changing the dispersion of the incoming wave. Hence, as the second sample, we dress our reference sample with circular periodic grooves. As can be seen in Fig. 3.2, the period of the grooves (p) is 16 mm and the thickness of the grooved metal (w) is 3.2 mm.

3.2.3 Sample 3: Coaxial Waveguide

Coaxial waveguides have a TEM_o mode without a cutoff. But the TEM mode cannot be excited with a linearly polarized incident beam. The dispersion relation for other propagating modes (TE, TM) of a coaxial waveguide is given by

$$k_z^2 = \frac{4\pi^2}{\lambda^2} - \frac{4\pi^2}{\lambda_c^2} \tag{3.1}$$

where λ_c is the cutoff wavelength of the mode. This cutoff for TE modes is approximately given by:

$$\lambda_{cTEm,1} = \frac{\pi(a+b)}{m} \tag{3.2}$$

where a and b are the outer and inner radii of the coaxial waveguide. For $k_z = 0$, the eigenwavelengths are equal to the cutoff wavelengths ($\lambda_{mode} = \lambda_c$).

Our coaxial waveguide (Sample 3) is identical to Sample 1 with a rod inside the hole. The diameter of the rod (b) is 6.6 mm and the length of the rod is 8 mm, the same as, the thickness of the metal blok (t). The rod sits in a hole of the same diameter as in reference sample (i.e. a=8 mm). The schematic of the sample is shown in Fig. 3.3.

3.2.4 Sample 4: Circular annular aperture with grooves

The last sample is the combination of the annular aperture (Sample 3) and the grooved structure (Sample 2). So, this is the sample that we call the sub-wavelength circular annular aperture surrounded by concentric periodic grooves (Fig. 3.4).

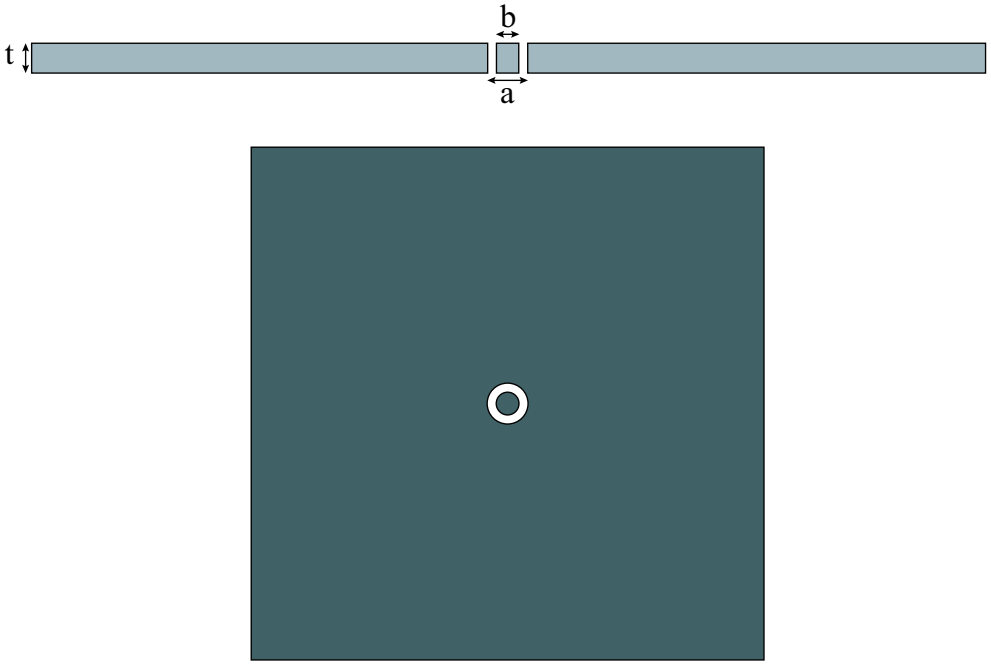

Figure 3.3: Schematic picture of Sample 3 with a=8 mm, t=8 mm and b=6.6 mm (Cross-sectional view on the top and front-view on the bottom).

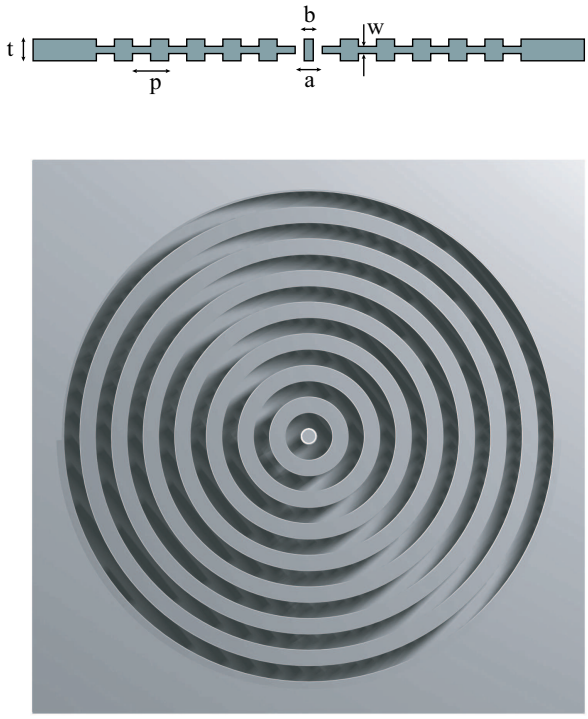

Figure 3.4: Schematic picture of Sample 4 with a=8 mm, b=6.6 mm, t=8 mm, p=16 mm and w=3.2 mm (Cross-sectional view on the top and front-view on the bottom).

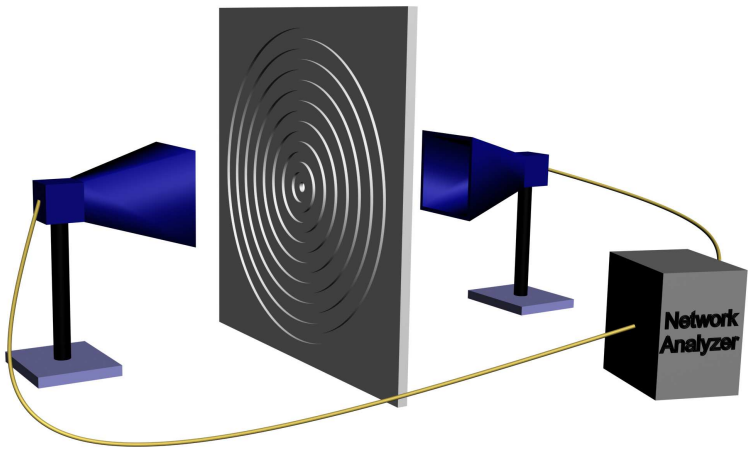

Figure 3.5: The experimental set up for transmission measurements.

3.3 Experimental and Theoretical Setup

3.3.1 Experimental Setup

The experimental setup comprises of an HP 8510C network analyzer and two standard gain horn antennas with a size of 42 mm $\times$ 60 mm to measure the transmission amplitude. The EM radiation is normally incident on the sample from a source antenna 15 cm away from the sample. The receiver antenna is 10 cm away from the sample. Fig. 3.5 illustrates the transmission setup.

3.3.2 Theoretical Setup

We setup the theoretical simulations using a commercial simulation software called CST Microwave Studio. This program solves Maxwell's equations in 3 dimensions with the FDTD (finite difference time domain) method.

The FDTD method is a direct space-time approach. In this method, an initial field is sent to the domain of calculations and its temporal and spatial evolution is analyzed [32].

To the first order, the derivative of a function of x can be approximated as:

$$\frac{d}{dx}f(x) \approx \frac{f(x+\triangle/2 - f(x-\triangle/2)}{\triangle} \tag{3.3}$$

In this equation $\triangle$ is assumed to be small. Maxwell's equations relate the components of the electric field and magnetic field. These components are functions of the spatial coordinates and time. Let us consider the Maxwell curl equations. Written in component form, we have six scalar equations. Here focus on two of them in particular:

$$\frac{\partial}{\partial t}H_x = -\frac{1}{\mu}\left\{\frac{\partial}{\partial z}E_y - \frac{\partial}{\partial y}E_z\right\} \tag{3.4}$$

$$\frac{\partial}{\partial t}E_y = -\frac{1}{\varepsilon}\left\{\frac{\partial}{\partial z}H_x - \frac{\partial}{\partial x}H_z\right\} \tag{3.5}$$

With the help of Eq. 3.3 can be approximated time and spatial derivatives appearing in these equations. But, in order to achieve useful results, these derivatives must be approximated in a special way. The algorithm due to Yee [33] is the most commonly used in approximating Eq. 3.4. The algorithm is explained in Fig. 3.6.

In the Yee algorithm, electric and magnetic field components are calculated at points shown in Fig. 3.6. The grid points are spaced $\triangle x$, $\triangle y$, and $\triangle z$ apart from each other. The electric and magnetic field components are then interlaced

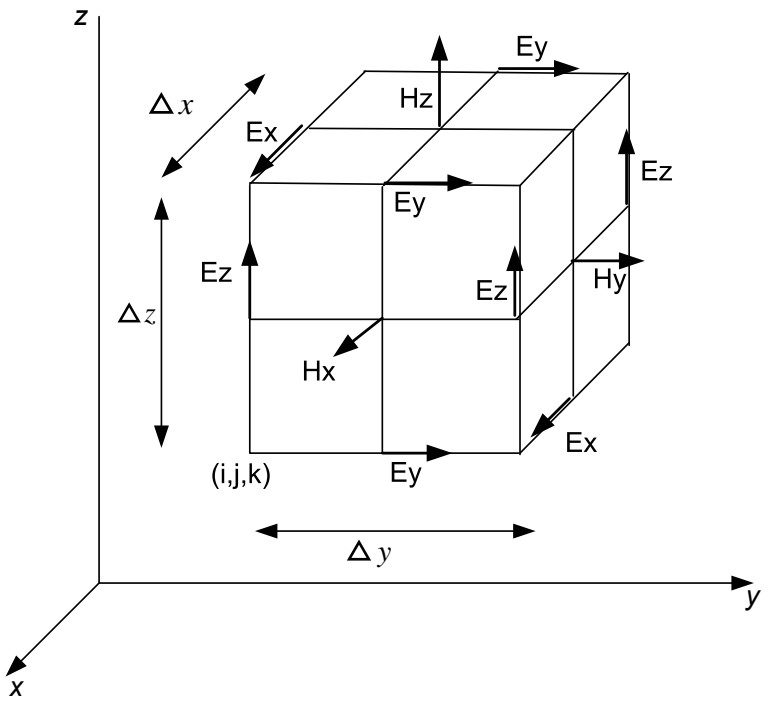

Figure 3.6: The grid on which the Yee algorithm is defined. It is known as the Yee cell. The magnetic field is calculated at points half-shifted with respect to the points at which the electric field is calculated.

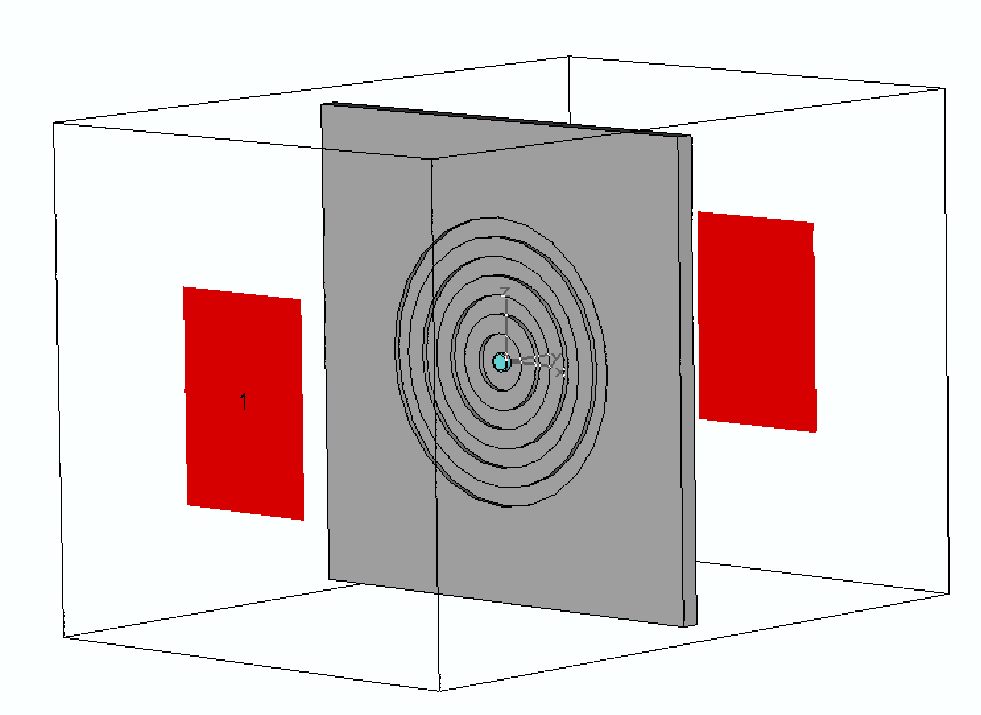

Figure 3.7: The simulation domain used for theoretical calculations.

in all three spatial dimensions. On the other hand, time is divided into steps of $\triangle t$. The electric field components are then computed at times $t = n \triangle t$, whereas the magnetic field components are calculated at times $t = (n + 1/2) \triangle t$.

Let us now write down the results for two particular components of the electric and magnetic fields. Here, the x component of the magnetic field can be written as

$$H^{n+1/2}_{x(i,j,k)} = H^{n-1/2}_{x(i,j,k)} + \frac{\triangle t}{\mu \triangle z} \left\{ E^{n}_{y(i,j,k)} - E^{n}_{y(i,j,k-1)} \right\} - \frac{\triangle t}{\mu \triangle y} \left\{ E^{n}_{z(i,j,k)} - E^{n}_{z(i,j,k-1)} \right\} \tag{3.6}$$

while the x component of the electric field can be written as

$$E^{n+1}_{x(i,j,k)} = E^{n}_{x(i,j,k)} + \frac{\triangle t}{\varepsilon \triangle y}\left\{H^{n+1/2}_{y(i,j+1,k)} - H^{n+1/2}_{y(i,j,k)}\right\} - \frac{\triangle t}{\varepsilon \triangle z}\left\{H^{n+1/2}_{z(i,j,k+1)} - H^{n+1/2}_{z(i,j,k)}\right\} \tag{3.7}$$

Looking at the form of Eqns. 3.6 and 3.7, we observe that once we know the electric field and the magnetic field at some point in time at all grid points, we can use the above equations to find the field components at later times.

In this method, an oscillating wave source is introduced and "directed" towards the structure to be analyzed (Fig. 3.7). The entire grid is then time-stepped until steady state response oscillations are obtained at all points on the grid. In order to use FDTD, a computational domain where the simulation will be performed must be established. The E and H fields will be determined at every point within this computational domain.

In our simulations, we used open boundary conditions and introduced ports as the transmitter and receiver antenna. The dimensions for the samples and ports distance were the same as those used in the experiment setup.

3.4 Enhanced Transmission

As explained in Chapter 2, SP modes can interact with the electromagnetic radiation on a metal surface with periodic corrugations. The coupling of incident EM radiation to the surface plasmon waves on the grating structure is given by:

$$k_{sp} = k_o + nk_g \tag{3.8}$$

Here k_{sp} is the SP wavevector, k_o is the portion of the incident wavevector that lies in the plane of the metal, n is an integer, and $k_g = 2\pi/p$ is the grating wave vector where p is the grating period. A resonance occurs when this condition is satisfied and the transmission is strongly enhanced compared to a smooth metal with a small aperture. SP wave vector is calculated using:

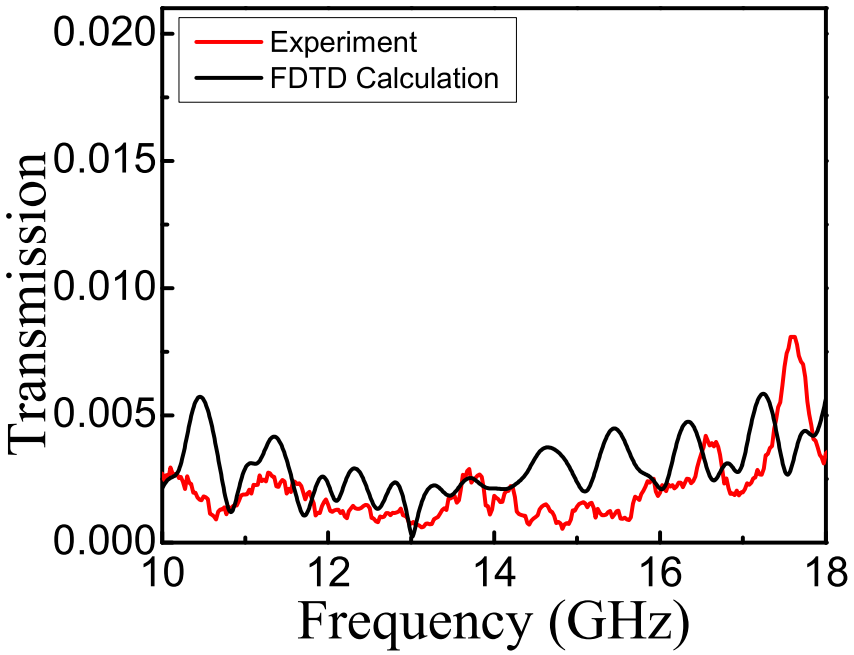

Figure 3.8: The transmission spectra calculated and measured for Sample 1. Here, the transmission was significantly below 0.0025.

$$k_{sp} = k_o \sqrt{\frac{\epsilon_m \epsilon_d}{\epsilon_m + \epsilon_d}} \tag{3.9}$$

where ϵ_m and ϵ_d denote the permittivity of metallic and dielectric media, respectively ($\epsilon_d = 1$ for air). For microwave frequencies, the permittivity of metals are high ($\sim 10^6$), compared to the permittivity of air; so $k_{sp} \cong k_o$ in the microwave range. Since the radiation is normally incident to the grating, the coupled wavevector should be integer multiples of k_g. These equations hold true for rectangular geometries such as hole arrays [4, 34] and square grating structures [13, 35]. The surface plasmon mode is different in cylindrical geometries. The studies by Ebbesen *et al.* and Lockyear *et al.* showed that this equation gives values for the surface plasmon mode of cylindrical geometries that are relatively close [12, 14].

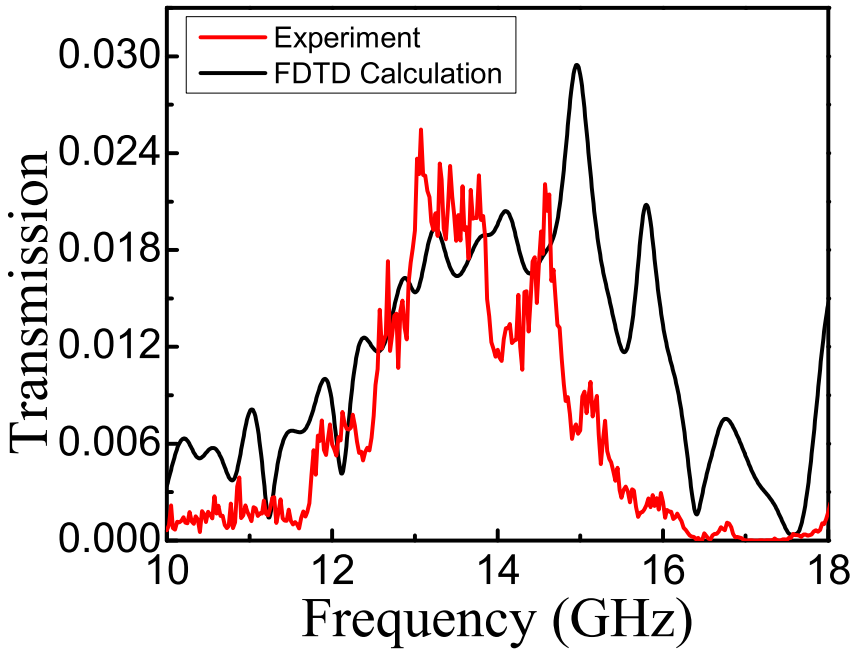

Figure 3.9: The transmission spectra calculated and measured for Sample 2. Between 12.9 and 14.0 GHz, there is a transmission peak with a transmission amplitude of 0.025.

The transmission spectra calculated and measured for Samples 1 and 2 are shown in Figs. 3.8 and 3.9, respectively. The experimental results are in good agreement with the FDTD calculations. For Sample 2, a transmission peak was measured between 12.9 and 14.0 GHz with a transmission amplitude of 0.025. But, for Sample 1, the transmission was below 0.0025. It can be easily seen that the transmission around 13 GHz is enhanced by coupling to the SPs. Figure 3.10 shows the enhancement of the transmission with respect to the reference sample (Sample 1). 20-fold enhancement was obtained around the SP resonance frequency with Sample 2.

The incident EM radiation is diffracted/scattered by the corrugation of the input surface and produces evanescent surface waves that tunnel through the hole,

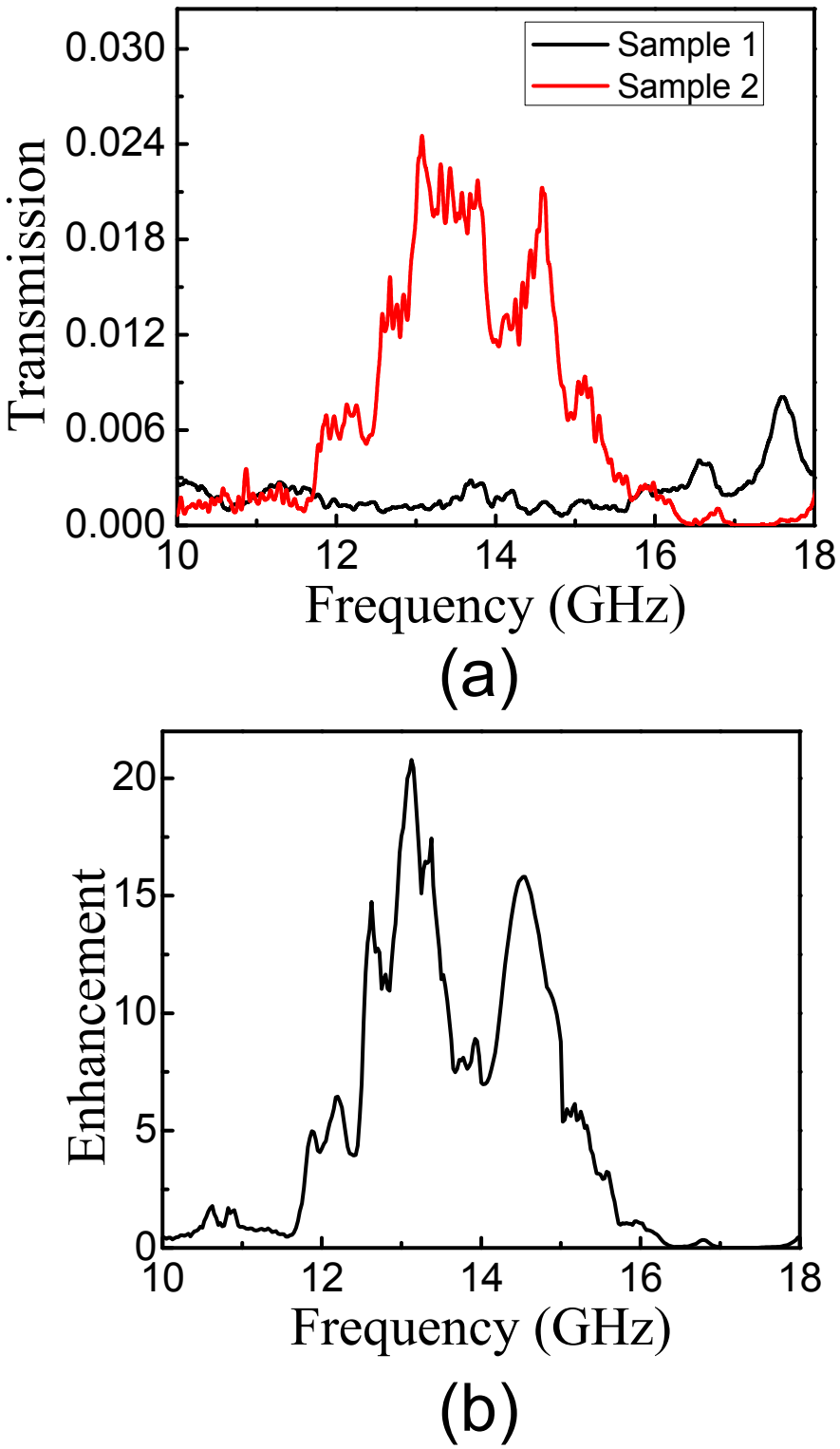

Figure 3.10: a) Comparison of transmission results for Sample 1 and 2. b) Enhancement factor obtained with Sample 2 with respect to Sample 1. 20-fold enhancement is obtained around the SP resonance frequency with Sample 2.

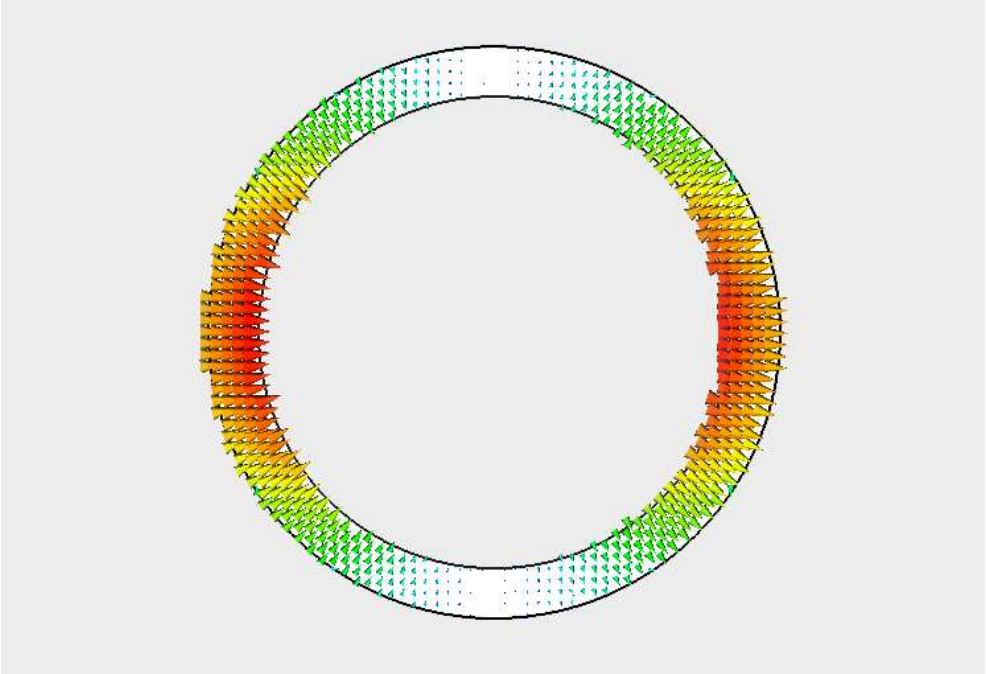

Figure 3.11: The electric field distribution of Sample 3 at resonance frequency (13.2 GHz). The direction of the field shows that this is a TE mode.

resulting in finite amplitude on the output side. Then, the evanescent waves again diffracted/scattered; the interference of the resulting waves leads to the radiation that propagates away from the structure. SPs act to enhance the fields associated with the evanescent waves, producing a way to increase the transmittance.

Transmission through an annular aperture (coaxial waveguide) was studied recently by Baida *et al.* [31]. It was shown theoretically that, at some wavelengths transmission through a coaxial waveguide was enhanced with respect to the circular aperture. In order to investigate the transmission through a coaxial waveguide, we use Sample 3. Coaxial waveguides have a TEM_o mode without a cutoff. Therefore, this structure is similar to a slit structure that can support a waveguide mode without a cutoff. However, the TEM mode cannot be excited with a linearly polarized incident beam.

We calculate the electric field distribution at 13.2 GHz (Fig. 3.11). It can be

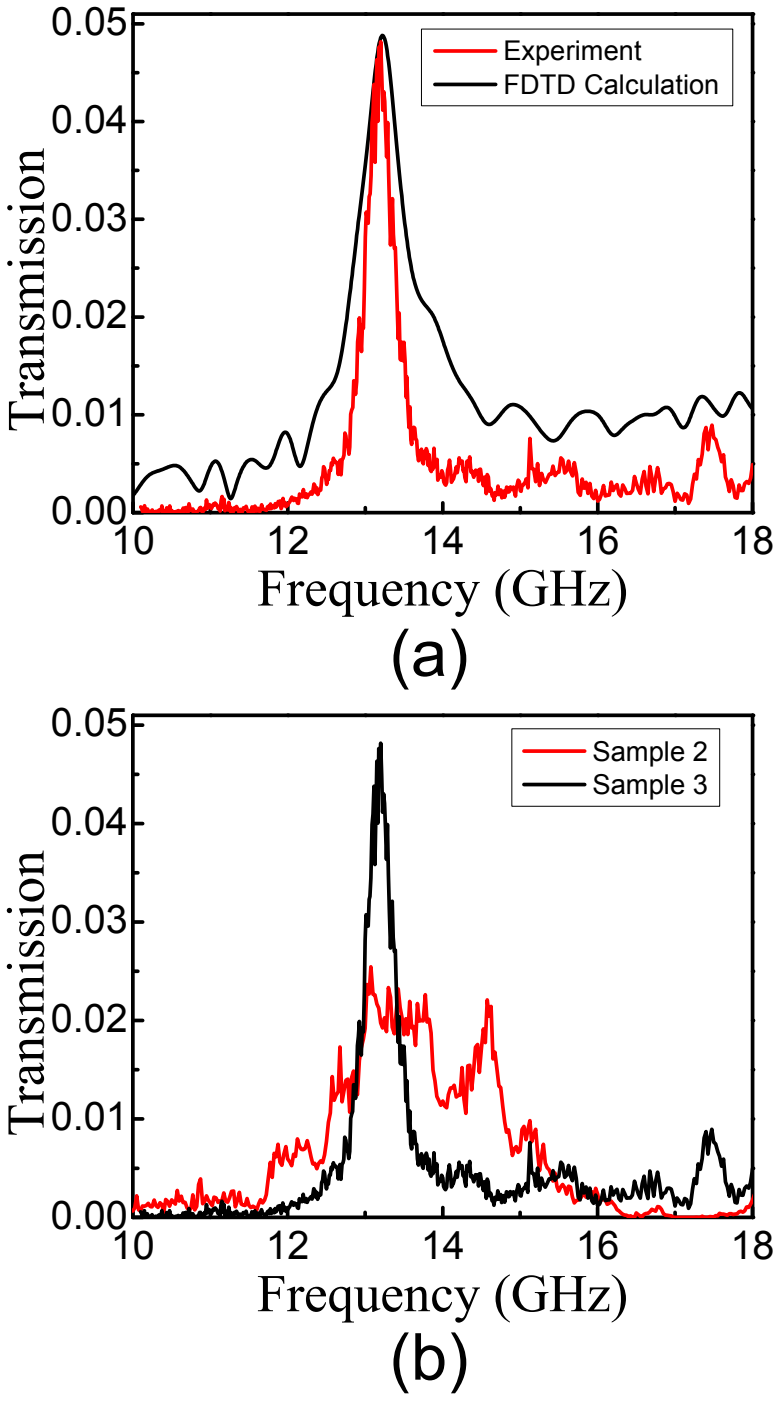

Figure 3.12: a) The transmission spectra calculated and measured for Sample 3. The transmission peak around 13 GHz and the transmission at this frequency is 0.05 b) Comparison of transmission results for Sample 2 and 3. The transmission peak obtained from Sample 3 is higher and narrower than the SP resonance peak obtained from Sample 2.

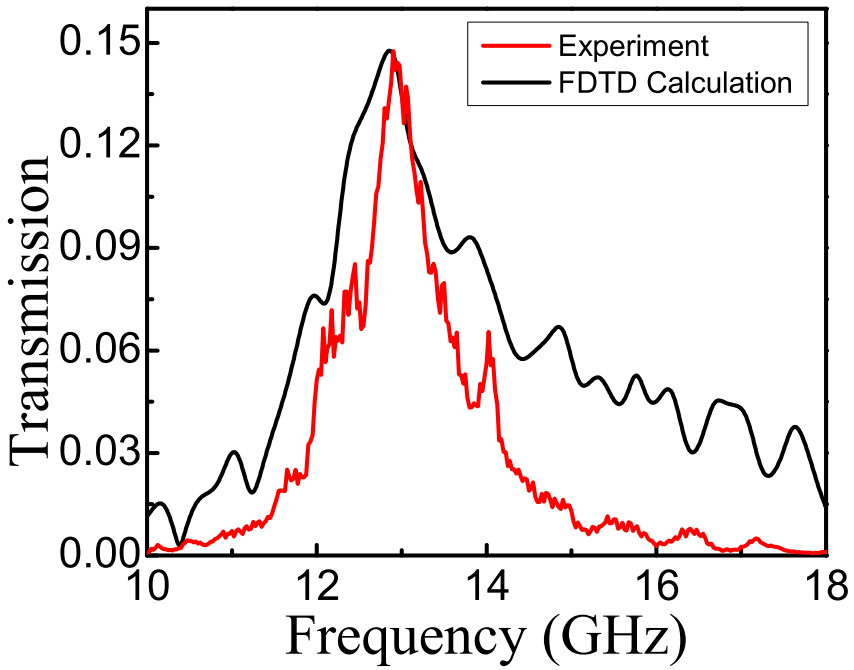

Figure 3.13: The transmission spectra calculated and measured for Sample 4. The transmission at the resonance frequency is 0.15, which was higher than those of Samples 2 and 3.

easily observed that the annular aperture has a TE mode at 13.2 GHz. Moreover, we measure the transmission through Sample 3 and these results agree well with the calculated results (Fig. 3.12(a)). As seen in Fig. 3.12(a), there is a transmission peak around 13 GHz and the transmission at this frequency is 0.05. Figure 3.12(b) shows that transmission at the TE mode frequency through Sample 3 and the transmission through Sample 2 at the SP resonance frequency. This comparison shows that, at the TE mode frequency, the transmission through Sample 3 is higher than the transmission through Sample 2 . In addition, the transmission peak of Sample 3 is narrower than the SP resonance frequency.

To obtain even higher transmission, we used the sample of annular aperture with periodic grooves (Sample 4). We expect a higher transmission from this

sample because, at the same frequency, both SP resonance due to the circular periodic grooves and TE mode due to the annular aperture are in play. The calculated and measured transmission (Fig. 3.13) of annular aperture surrounded by concentric periodic grooves shows extraordinary high transmission at 12.9 GHz (23.25 mm) as expected. The transmission through Sample 4 at this frequency is 0.15 and higher than the those of Samples 2 and 3. The transmission peak is narrower than that achieved with Sample 2, but wider than that obtained with Sample 3. In Fig. 3.14, the enhancement spectra obtained with Sample 4 with respect to Sample 1 is presented. A maximum enhancement factor of 145-fold was obtained at the resonance frequency. Compared to Sample 2, there is a 7.5 fold increment in enhancement factor. Also, note that the area of the hole in Sample 1 is $16\pi^2$ and in Sample 4 this hole area is reduced by a factor of 3.13 with respect to Sample 1. If we include the reduction in the area of the aperture, a 450-fold enhancement is obtained through the subwavelength annular aperture. The combination of SP resonance and TE mode resonance at the same frequency enable us to achieve such a high transmission.

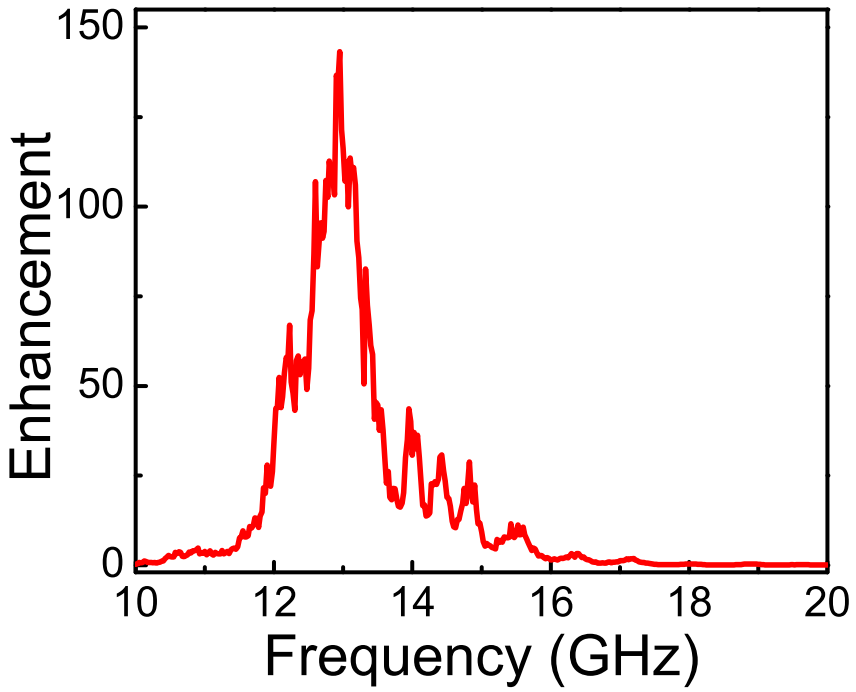

Figure 3.14: The transmission enhancement factor obtained with Sample 4 with respect to Sample 1. A maximum enhancement factor of 145-fold is obtained at the resonance frequency.

Chapter 4

Beaming of Electromagnetic Waves

4.1 Introduction

The transmission of electromagnetic (EM) waves through a single subwavelength aperture has been studied for many years. As defined in the standard diffraction theory by Bethe [36] in 1944, a circular aperture with a subwavelength diameter transmits EM waves rather poorly $\sim (d/\lambda)^4$ and exiting EM waves are fully diffracted in all directions. These two disadvantages of low transmission and diffraction are the main problems of manipulating light, especially at the subwavelength scales. However, it has been shown that not only the enhancement of the transmission but also the confinement of the transmitted beam is possible by surrounding the metal surface of the subwavelength apertures with periodic corrugations [12].

The use of SPs helps us to concentrate light in subwavelength structures that is obtained with different permittivities of the metal and the surrounding media. Beaming of light through a single aperture with periodic surface corrugations around the aperture were shown experimentally and studied theoretically [12, 13, 17]. It was also shown theoretically that it is possible to optimize the angular

confinement using a subwavelength circular coaxial aperture with a surrounding array of grooves [29]. In the previous chapter, we presented a circular annular aperture with periodic grooves that optimizes the transmission. In this chapter, we will present the near-field and far-field distributions of EM waves emitted from subwavelength circular annular apertures and circular annular apertures surrounded by concentric periodic grooves. We will demonstrate the angular dependence of the beams transmitted through our samples. We will show that it is also possible to confine the beam transmitted through subwavelength circular annular aperture with periodic grooves.

4.2 Experimental Setup

In the experimental setup for angular distribution measurements the receiver antenna is placed 50 cm (22λ) away from the sample's back side and was connected to a rotating arm to measure the angular dependence of the far-field radiation (Fig 4.1). We change the angle of the receiver antenna with the help of rotating arm. We have 1^0 resolution in this experimental setup.

For the scanning experiments, we replace the receiver antenna with a monopole antenna. The monopole source is obtained by removing 0.5 cm of the cladding from a coaxial cable and leaving the metal part as shown in Fig. 4.2. We vary the distance of the monopole antenna with an x-y stage, starting from the surface of the sample. However, because of the finite size of the monopole we are able to start scanning only 4 mm away from the Sample surface. The details of the experimental setup used to scanning measurements are summarized in Fig. 4.3.

4.3 Near-field EM distributions

As explained previously, the enhancement of the transmission refer to the surface plasmons waves on the surface. In addition, surface waves have their maximum

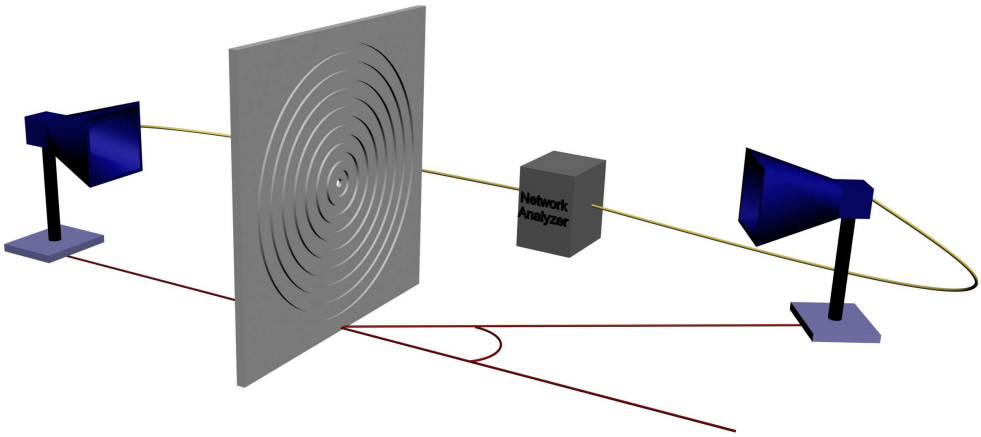

Figure 4.1: The experimental setup used in angular distribution measurements.

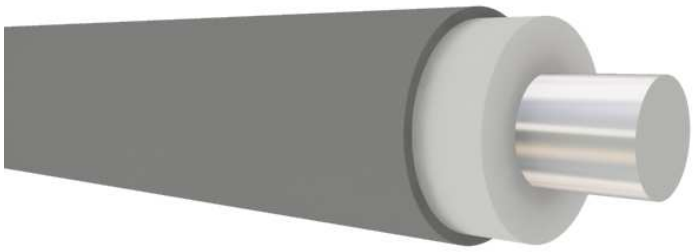

Figure 4.2: The monopole antenna obtained by removing the outer jacket of a coaxial cable.

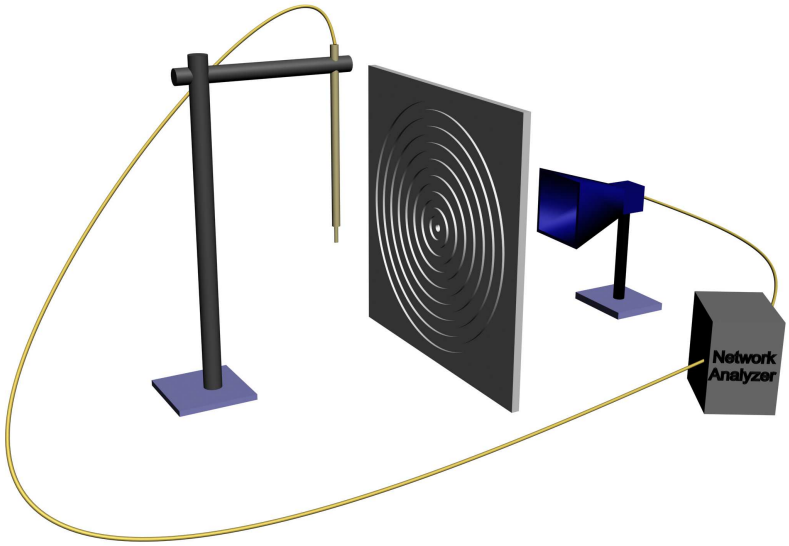

Figure 4.3: The experimental setup used in scan measurements.

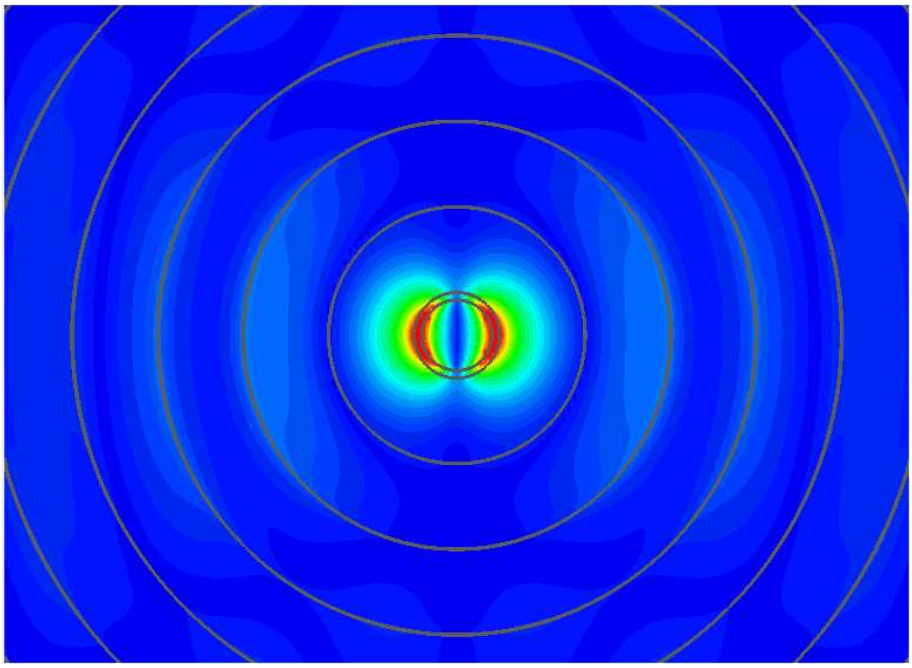

Figure 4.4: Electric field distribution calculated on the surface of Sample 4 at the resonance frequency (13 GHz).

electric field values on the surface and exponentially decay away from the surface. Figure 4.4 shows the electric field distribution calculated on the surface of Sample 4 at the resonance frequency (12.9 GHz). The waves on the surface of the sample can be observed.

In order to observe these surface waves, we scan the output surface of Sample 2. Due to the restriction of the experimental set up, we are able to scan only 4 mm away from the surface. Figure 4.5(a) shows the field calculated on the output surface of Sample 2, where the dotted lines refer to the aperture surface. The field is both calculated and measured on a plane 4 mm away from the output surface of Sample 2 and is shown in Fig. 4.5(b). The full-width at half maximum (FWHM) of the measured field is equal to 9 mm ($\simeq \lambda/2.5$) . The subwavelength FWHM suggests the existence of the evanescent field at this distance.

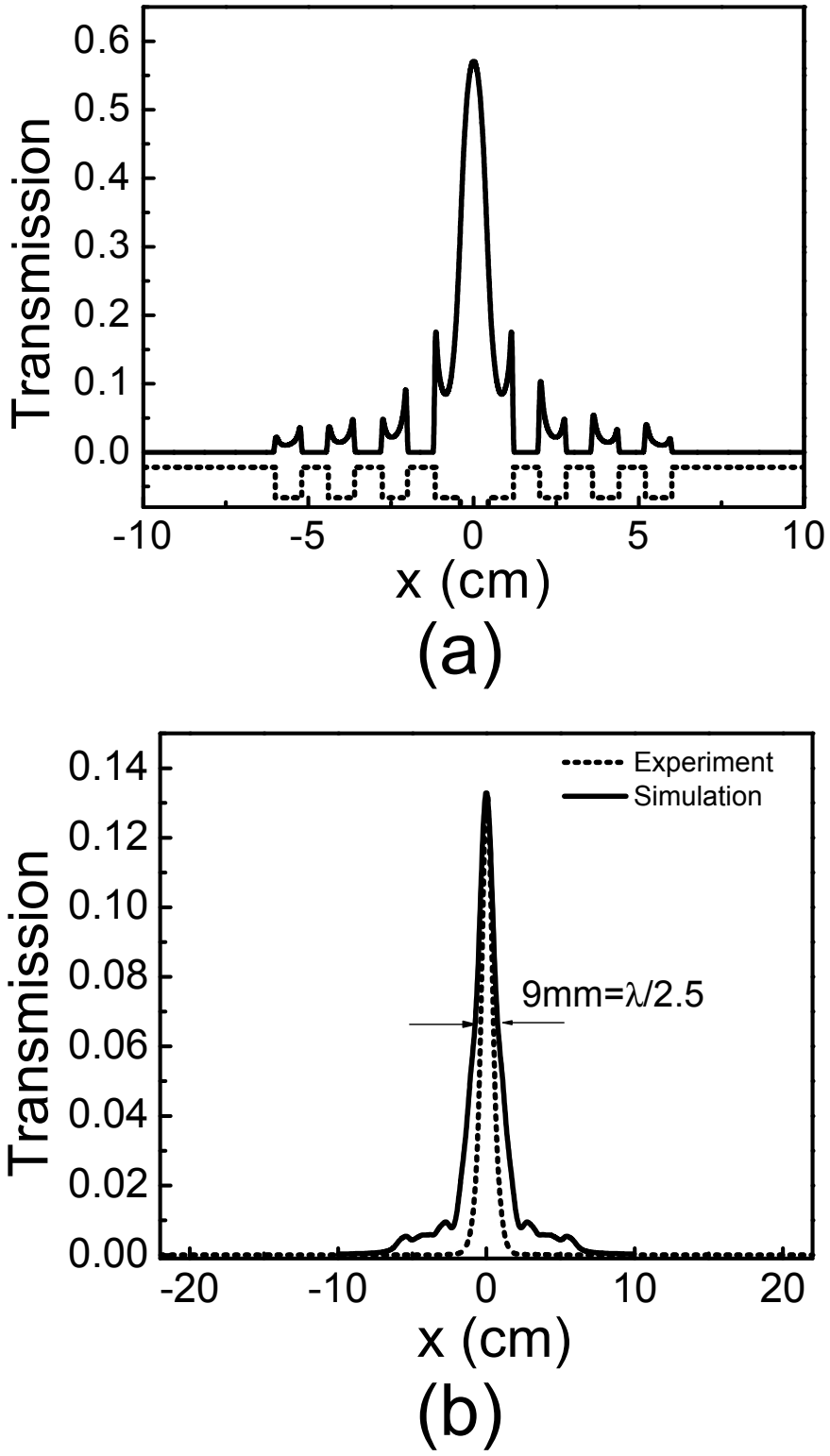

Figure 4.5: a) The transmitted field calculated on the output surface of Sample 2. b) The measured and calculated fields 4 mm away from the surface of Sample 2.

4.4 Far-field EM distributions

We measure and calculate the far-field angular distributions for our four samples. Figure 4.6 shows the normalized measured and calculated angular transmission distribution at the resonance frequency for Sample 1 and 2. The angular divergence of the beam transmitted through Sample 1 is $\pm 12^o$, whereas the that of the beam that emerges from Sample 2 is $\pm 3^o$. Although, in both sample electromagnetic waves transmitted from a subwavelength aperture, the angular divergence of the beam transmitted through Sample 2 reduced four-fold compared to the that of Sample 1.

The angular transmission intensity distribution at the enhanced transmission frequency (13 GHz) for Samples 3 and 4 is presented in Fig. 4.7. FWHM divergence of the beam is $\pm 12^o$ and $\pm 3^o$ for Samples 3 and 4, respectively. The angular divergence of the beam transmitted through Sample 3 is very similar to the beam transmitted through Sample 1. Moreover, the angular divergence of the beam transmitted through Sample 2 is very similar to the beam transmitted through Sample 4. Hence, there is an angular confinement for the beams transmitted from grooved samples; the confinement can be attributed to the grooves on the surface of samples.

The EM radiation emerging from the groove structure is transmitted through a subwavelength aperture like the radiation emerging from non-grooved samples. It is intuitively expected that the transmitted EM waves would quickly diffract in all directions due to the subwavelength dimensions of the aperture [36]. On the contrary, we observed that the transmitted EM waves are confined to a narrow spatial region when the subwavelength aperture is surrounded by periodic circular grooves. The surface wave momentum and the momentum of the corrugation around the subwavelength aperture limit the allowed range of momentum of the re-radiated EM waves. The circular symmetry of the structure suggests that the off-axis beams are suppressed due to the destructive interference. In addition, the beams that are normal to the surface of the aperture constructively interfere since the beams transmitted through the hole and grooves are in phase. This constructive interference enables the confinement of the beam with the grooved

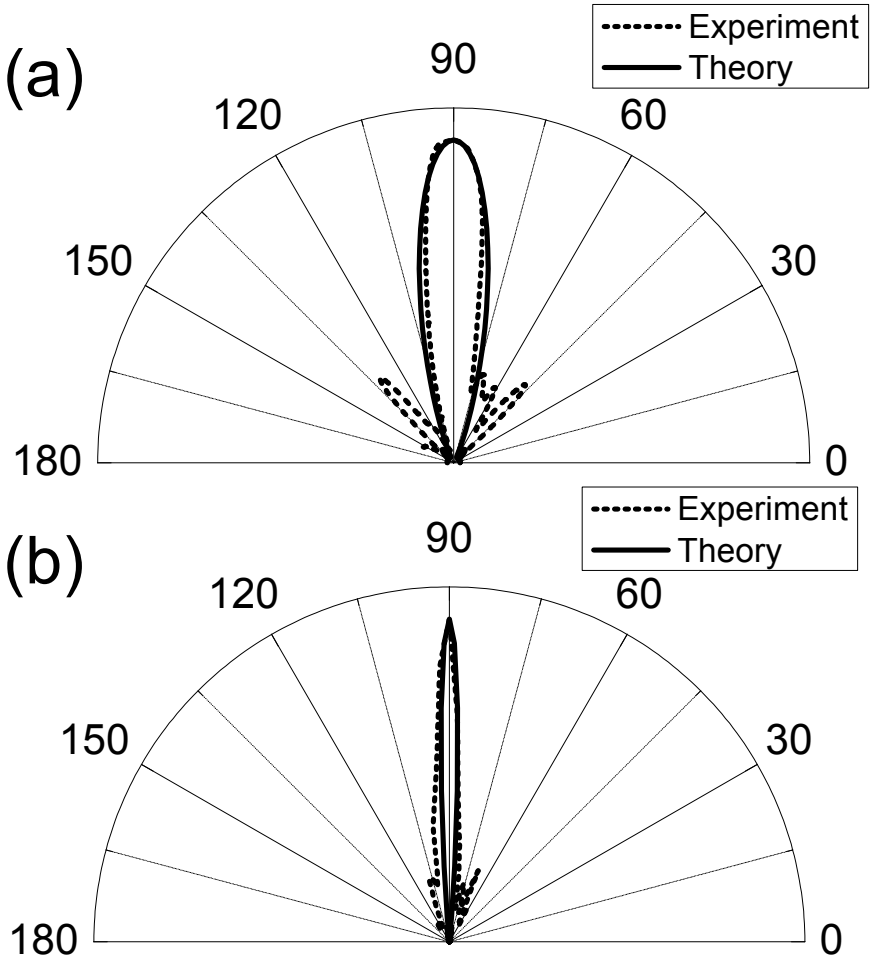

Figure 4.6: Normalized angular transmission distribution for a) Sample 1 and b) Sample 2 at the resonance frequency (13 GHz).

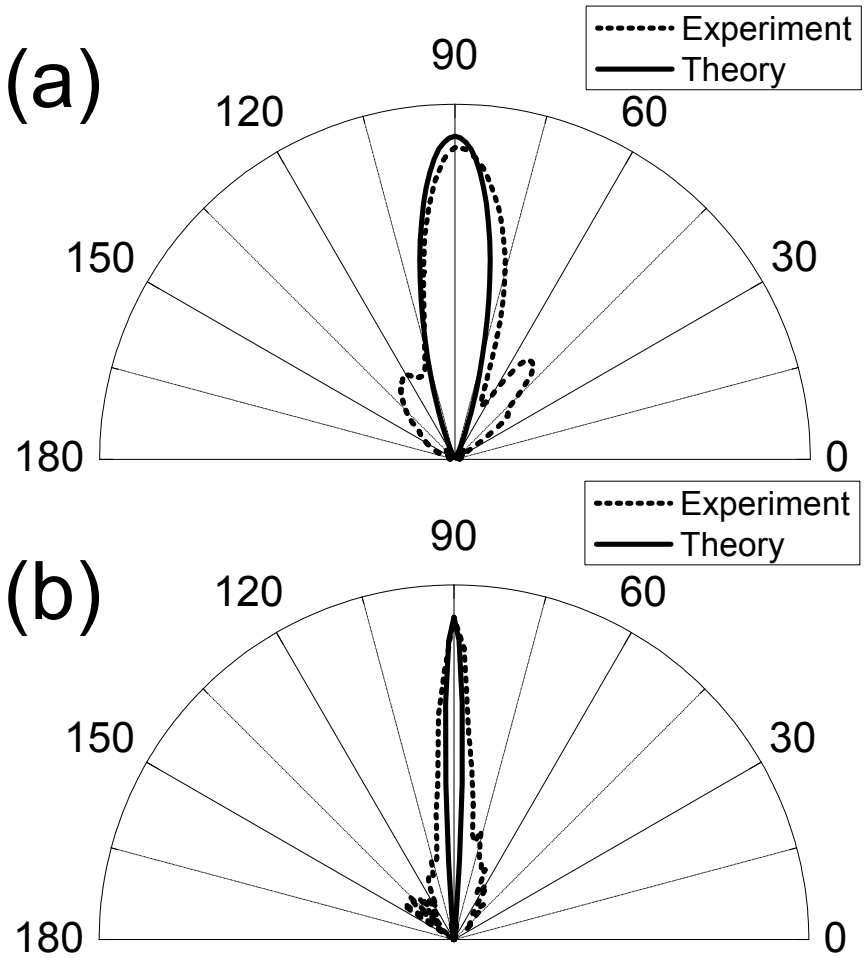

Figure 4.7: Normalized angular transmission distribution for a) Sample 3 and b) Sample 4 at the resonance frequency (13 GHz).

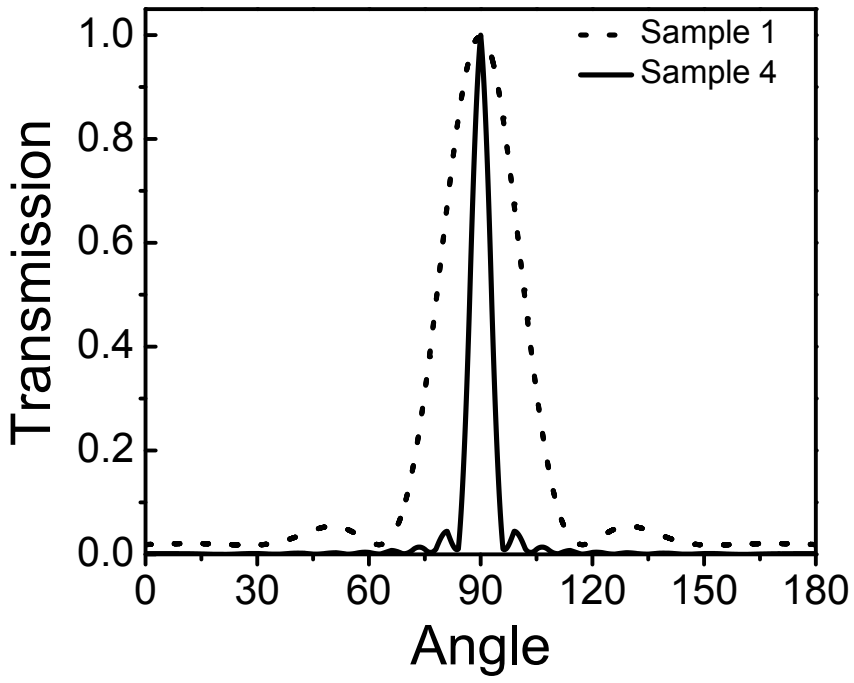

Figure 4.8: Comparison of the far-field results calculated for Samples 1 and 4.

samples.

The comparison of the far-field distributions of EM waves calculated for Sample 1 and 4 is presented in Fig. 4.8. The FWHM divergence of the beam calculated for Samples 1 and 4 is $\pm 12^o$ and $\pm 3^o$, respectively, in agreement with the measurements. Sample 4 optimizes the angular divergence of the beam since FWHM of the beam is reduced four-fold compared to the beam transmitted through a subwavelength aperture (Sample 1). Although we can achieve a higher transmission with Sample 4 with respect to Sample 2, we cannot achieve a more confined beam with Sample 4 with respect to Sample 2. The reason for this is possibly that: we achieved the limit of the angular confinement with such a structure.

The electric field intensity distribution for Sample 1 is presented in Fig. 4.9(a). As explained in the introduction part of this chapter, the electric field intensity diffracts quickly. In Fig. 4.9(b), the electric field distribution of the transmitted

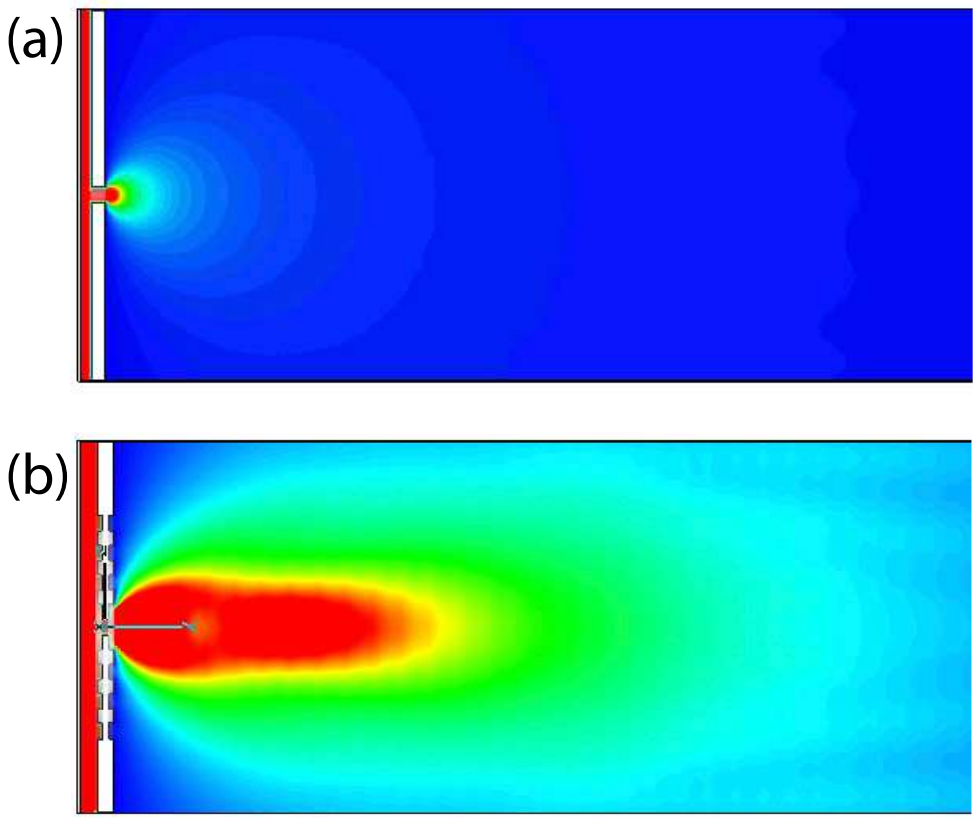

Figure 4.9: The electric field distribution calculated for (a) Sample 1 and (b) Sample 4. Sample 4 optimizes the angular divergence of the beam since FWHM divergence of the beam is reduced four-fold compared to the beam transmitted through a subwavelength aperture (Sample 1).

beam calculated for Sample 4 at the resonance frequency is presented. Figure 4.10 shows the electric field intensity measured at the resonance frequency and off-resonance frequency over a region of a 44 cm $\times$ 90 cm area. The electric field intensity measured on the output side of the aperture is recorded with a monopole antenna (Fig. 4.2) with a resolution of 0.5 cm with our scanning experimental setup. Our experiment shows that the electric field intensity transmitted through Sample 4 is confined to a narrow spatial region and propagates without diffracting into a wide angular region at the resonance frequency. On the other hand, at the non-resonance frequency the electric field intensity is diffracted quickly to a broad area. The theoretical results are in good agreement with the experimental results.

Last, we investigate which surface is responsible for the beaming effect and design a circular aperture with grooves on only one of sides of the metal block. The angular distributions of EM waves transmitted through different sides are shown in Fig. 4.11. These results show that when we illuminate the sample on the side of a grooved surface (no grooves on the exit surface), we could not observe a beaming effect. On the other hand, when the sample is illuminated on the side of the flat surface such that the output surface is grooved, a beaming effect occurs. This can be interpreted as only the output surface being responsible for the beaming effect.

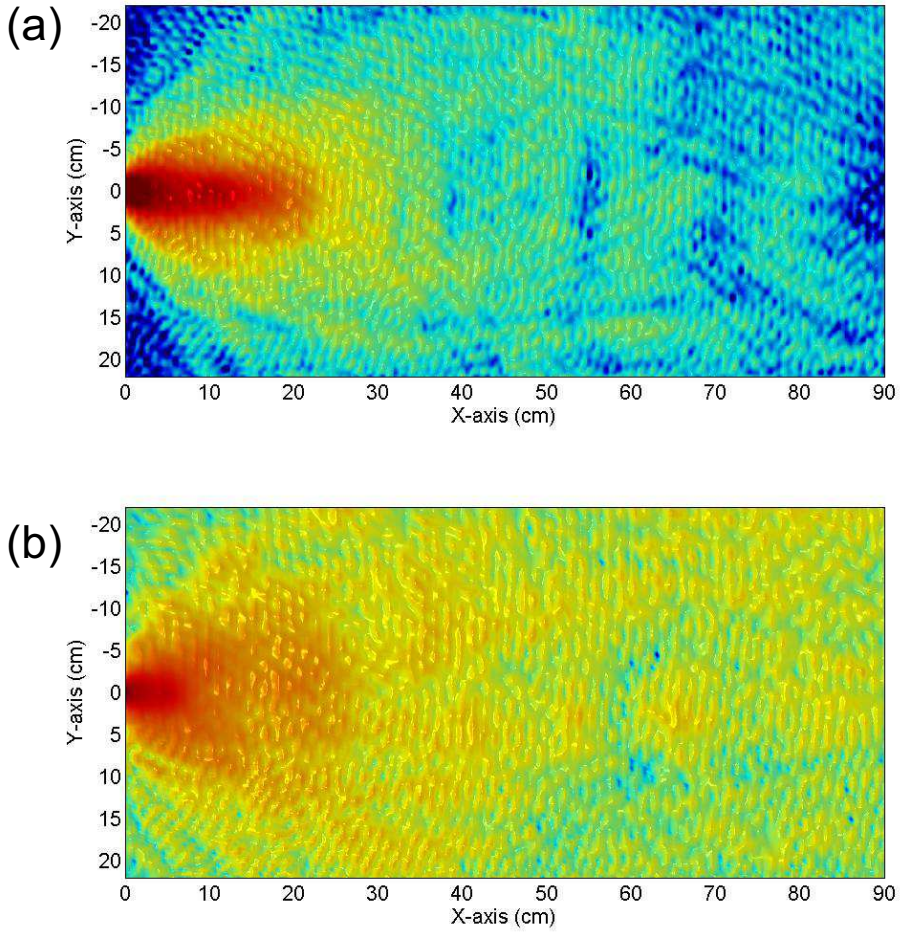

Figure 4.10: (a) The electric field distribution measured for Sample 4 at the resonance frequency (b) The electric field distribution measured for Sample 4 at the non-resonance frequency.

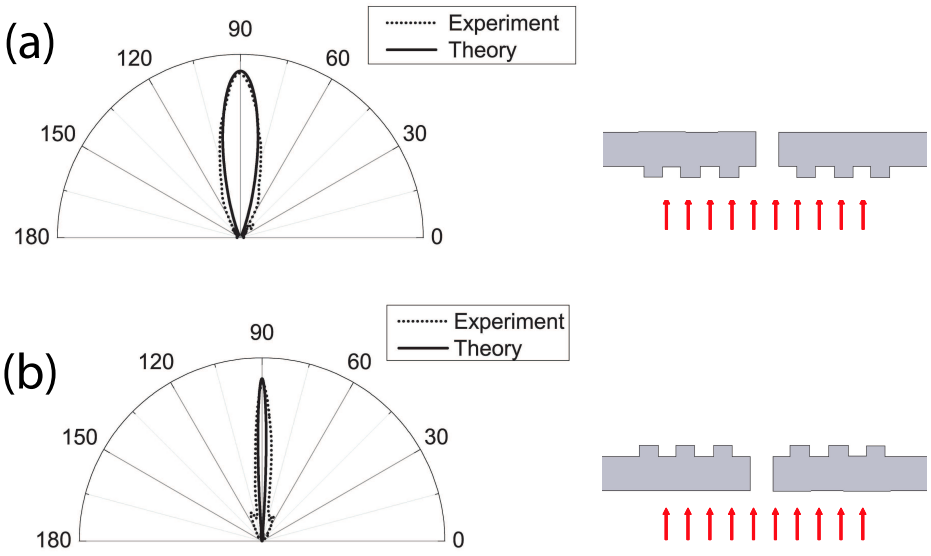

Figure 4.11: Normalized angular transmission distribution for one-sided grooved samples at the resonance frequency.

Chapter 5

Conclusions and Future Work

This chapter includes a brief summary of the previous chapters and the results of this thesis work. In addition, we briefly state new questions and possible future work that our results lead us to.

In the second chapter, we had a discussion about the theory of surface plasmons and excitation of surface plasmons. We discussed that surface plasmons propagate along the metal-dielectric interface. SPs are non-radiative surface waves so it is needed to use some techniques to excite SPs. We presented three different methods to excite SPs. In this work, we used the grating coupled method to excite SPs.

The main objective of this thesis work can be stated as the investigation of the coupling mechanism between microwave radiation and surface plasmons in 2-D metallic grating structures. We demonstrated an enhanced transmission through subwavelength apertures surrounded by the grooves. 20-fold transmission enhancement was measured around the SP resonance frequency for the subwavelength circular aperture with circular periodic grooves. We also studied structures with circular annular aperture. Our results show that high transmission through a circular annular aperture is assisted by the guided mode of the coaxial waveguide. Moreover, a remarkable 145-fold enhancement of transmission was observed

with a subwavelength circular annular aperture surrounded by concentric periodic grooves via coupling to the SPs and the guided mode of annular aperture. These results were verified by our FDTD calculations.

Furthermore, we presented near-field and far-field EM distributions measured and calculated for subwavelength circular annular apertures with and without concentric periodic grooves in the microwave regime. We showed that the beam transmitted through circular apertures surrounded by concentric periodic grooves has a subwavelength FWHM near the aperture. In addition, we measured the distributions normalized angular transmission through these apertures. The angular divergence of the beam transmitted from the circular annular apertures surrounded by concentric grooves (Sample 4) is four-fold reduced compared to the beam transmitted through a subwavelength aperture (Sample 1). To sum up, our transmission experiments showed that periodic surface corrugation led to an enhanced transmission and beaming around the SP resonance frequency, which was determined by the groove periodicity. The coupling of EM waves to the SPs and the guided mode of annular aperture can explain these effects.

The results of this thesis work lead us to some interesting questions. For instance, is it possible to use these apertures as a microwave scanning probe and achieve a subwavelength resolution? Another interesting question is, how to attain a Bessel beam through these apertures? We will attempt to answer these questions in our future work. For future research directions, the ultimate goal should also be to move this work toward optical wavelengths.

Bibliography

[1] V. M. Agranovich and D. L. Mills, *Surface Polaritons: Electromagnetic Waves at Surfaces and Interfaces*, North-Holland, Amsterdam, 1992.

[2] H. Raether, *Surface Plasmons on Smooth and Rough Surfaces and on Gratings*, Springer-Verlag, Berlin, 1988.

[3] W. L. Barnes, A. Dereux, and T. W. Ebbesen, "Surface plasmon subwavelength optics," *Nature* **424**, pp. 824–830, 2003.

[4] T. W. Ebbesen, H. J. Lezec, H. F. Ghaemi, T. Thio, and P. Wolf, "Extraordinary optical transmission through subwavelength hole arrays," *Nature* **39**, pp. 667–669, 1998.

[5] D. E. Grupp, H. J. Lezec, T. W. Ebbesen, K. M. Pellerin, and T. Thio, "Crucial role of metal surface in enhanced transmission through subwavelength apertures," *Appl. Phys. Lett.* **77**, pp. 1569–71, 2000.

[6] F. J. Garcia-Vidal, H. J. Lezec, T. W. Ebbesen, and L.Martin-Moreno, "Multiple paths to enhance optical transmission through a single subwavelength slit," *Phys. Rev. Lett.* **90**, p. 213901, 2003.

[7] F. J. Garcia-Vidal, L. Martin-Moreno, H. J. Lezec, and T. W. Ebbesen, "Focusing light with a single subwavelength aperture flanked by surface corrugations," *Appl. Phys. Lett.* **83**, pp. 4500–4502, 2003.

[8] W. Liu and D. P. Tsai, "Optical tunneling effect of surface plasmon polaritons and localized surface plasmon resonance," *Phys. Rev. B* **65**, pp. 155423–1–155423–6, 2002.

[9] J. A. Porto, F. J. Garcia-Vidal, and J. B. Pendry, "Transmission resonances on metallic gratings with very narrow slit," *Phys. Rev. Lett.* **83**, pp. 2845–48, 1999.

[10] X. Shi and L. Hesselink, "Mechanisms for enhancing power throughput from planar nano-apertures for near-field optical data storage," *J. Appl. Phys.* **41**, pp. 1632–1635, 2002.

[11] U. Schröter and D. Heitmann, "Surface-plasmon-enhanced transmission through metallic gratings," *Phys. Rev. B* **58**, pp. 15419–21, 1999.

[12] H. J. Lezec, A. Degiron, E. Devaux, R. A. Linke, L. Martin-Moreno, F. J. Garcia-Vidal, and T. W. Ebbesen, "Beaming light from a subwavelength aperture," *Science* **297**, pp. 820–22, 2002.

[13] S. S. Akarca-Biyikli, I. Bulu, and E. Ozbay, "Enhanced transmission of microwave radiation in one-dimensional metallic gratings with subwavelength aperture," *Appl. Phys. Lett.* **85**, p. 1098, 2004.

[14] T. Thio, K. M. Pellerin, R. A. Linke, H. J. Lezec, and T. W.Ebbesen, "Enhanced light transmission through a single subwavelength aperture," *Opt. Lett.* **26**, p. 1972, 2001.

[15] E. Popov, M. Neviere, S. Enoch, and R. Reinisch, "Theory of light transmission through subwavelength periodic hole arrays," *Phys. Rev. B* **62**, pp. 16100–08, 2000.

[16] L. Martin-Moreno, F. J. Garcia-Vidal, H. J. Lezec, K. M. Pellerin, T. Thio, J. B. Pendry, and T. W. Ebbesen, "Theory of extraordinary optical transmission through subwavelength hole arrays," *Phys. Rev. Lett.* **86**, pp. 1114–17, 2001.

[17] M. J. Lockyear, J. R. A. P. Hibbins, and C. R. Lawrence, "Surface-topography-induced enhanced transmission and directivity of microwave radiation through a subwavelength circular metal aperture," *Appl. Phys. Lett.* **84**, p. 2040, 2004.

[18] L. Martin-Moreno, F. J. Garcia-Vidal, H. J. Lezec, A. Degiron, and T. W. Ebbesen, "Theory of highly directional emission from a single subwavelength aperture surrounded by surface corrugations," *Phys. Rev. Lett.* **90**, p. 167401, 2003.

[19] H. Caglayan, I. Bulu, and E. Ozbay, "Extraordinary grating-coupled microwave transmission through a subwavelength annular aperture," *Opt. Express* **13**, pp. 1666–1671, 2005.

[20] H. Caglayan, I. Bulu, and E. Ozbay, "Beaming of electromagnetic waves emitted through a subwavelength annular aperture," *J. Opt. Soc. Am. B* .

[21] C. Kittel, *Introduction to Solid State Physics*, John Wiley and Sons, New York, 1996.

[22] T. Thio, H. Lezec, T. Ebessen, K. M. Pellerin, G. D. Lewen, A. Nahata, and R. A. Linke, "Giant optical transmission of sub-wavelength apertures: physics and applications," *Nanotechnology* **13**, pp. 429–432, 2002.

[23] J. M. Steele, C. E. Moran, A. Lee, C. M. Aguirre, and N. J. Halas, "Metallodielectric gratings with subwavelength slots: Optical properties," *Phys. Rev. B* **68**, p. 205103, 2003.

[24] N. Bonod, S. Enoch, L. Li, P. Evgeny, and M. Neviere, "Resonant optical transmission through thin metallic films with and without holes," *Opt. Express* **11**, pp. 482–490, 2003.

[25] A. G. Borisov, F. J. G. de Abajo, and S. V.Shabanov, "Role of electromagnetic trapped modes in extraordinary transmission in nanostructured materials," *Phys. Rev. B* **71**, p. 075408, 2005.

[26] S. S. Akarca-Biyikli, I. Bulu, and E. Ozbay, "Resonant excitation of surface plasmons in one-dimensional metallic grating structures at microwave frequencies," *J. Opt. A: Pure Appl. Opt.* **7**, pp. 159–164, 2005.

[27] M. J. Lockyear, A. P. Hibbins, J. R. Sambles, and C. R. Lawrence, "Enhanced microwave transmission through a single subwavelength aperture surrounded by concentric grooves," *J. Opt. A: Pure Appl. Opt.* **7**, pp. 152–158, 2005.

[28] U. C. Fischer and M. Zapletal, "The concept of a coaxial tip as a probe for scanning near field optical microscopy and steps towards a realisation," *Ultramicroscopy* **42-44**, pp. 393–398, 1992.

[29] F. I. Baida and D. V. Labeke, "Light transmission by subwavelength annular aperture arrays in metallic films," *Opt. Comm.* **209**, pp. 17–22, 2002.

[30] F. I. Baida, D. V. Labeke, G. Granet, A. Moreau, and A. Belkhir, "Origin of the super-enhanced light transmission through a 2-d metallic annular aperture array: a study of photonic bands," *Appl. Phys. B* **79**, pp. 1–8, 2004.

[31] F. I. Baida, D. V. Labeke, and B. Guzial, "Enhanced confined light trasmission by single subwavelength apertures in metallic films," *Appl. Opt.* **42**(34), p. 6811, 2003.

[32] A. Taflove, *Computational Electrodynamics: The Finite-Difference Time-Domain Method*, Artech House INC, Norwood, 1995.

[33] K. Yee, "Numerical solution of inital boundary value problems involving maxwell's equations in isotropic media," *IEEE Trans. Antennas Propag.* **14**, p. 302, 1966.

[34] H. F. Ghaemi, T. Thio, D. E. Grupp, T. W.Ebbesen, and H. J. Lezec, "Surface plasmons enhance optical transmission through subwavelength holes," *Phys. Rev. B* **58**, p. 6779, 1998.

[35] A. P. Hibbins, J. R. Sambles, and C. R. Lawrence, "Grating-coupled surface plasmons at microwave frequencies," *J. Appl. Phys.* **86**(4), p. 1791, 1999.

[36] H. A. Bethe, "Theory of diffraction by small holes," *Phys. Rev.* **66**, p. 163182, 1944.